

Scalable and Distributed Silhouette Approximation

Ilie Sarpe

ilsarpe@kth.se

KTH Royal Institute of Technology

Federico Altieri

altierif87@gmail.com

University of Padova

Andrea Pietracaprina

capri@dei.unipd.it

University of Padova

Geppino Pucci

geppo@dei.unipd.it

University of Padova

Fabio Vandin

fabio.vandin@unipd.it

University of Padova

Abstract

The *silhouette* is one of the most widely used measures to assess the quality of a k -clustering of a dataset of n elements. Its popularity stems from the fact that its evaluation requires no information beyond the clustering assignment. In addition, the silhouette is extremely easy to interpret, with a plethora of applications in various domains. The silhouette provides a score to measure the quality of a clustering as a whole or for each individual element. However, the exact computation of the: (i) silhouette of each element of a dataset; and (ii) the global silhouette of the entire clustering; require $\Theta(n^2)$ distance calculations, under general metrics. The quadratic complexity $\Theta(n^2)$ is extremely prohibitive, especially on massive modern datasets. Surprisingly, existing approximate methods using $O(n^2)$ distance calculations are heuristics and do not offer *provable* and *controllable* guarantees on the quality of their results.

In this work, we introduce the first rigorous and efficient algorithms to estimate: (i) the (local) silhouette of each element of a dataset; and (ii) the (global) silhouette; of any metric k -clustering. Our methods are based on sampling, performing $O(nk\varepsilon^{-2} \ln(nk/\delta))$ distance computations, and providing estimates with additive error $O(\varepsilon)$ with probability at least $1 - \delta$. That is, the user-defined parameters ε and δ in $(0, 1)$ control the trade-off between accuracy and efficiency. Furthermore, we introduce a scalable and *distributed* design of our methods for the MapReduce and Massively Parallel Computing (MPC) frameworks. Our distributed algorithms require a constant number of rounds and sublinear local memory, under practical parameter setting. Finally, we perform extensive experiments to compare our methods with state-of-the-art approaches. The results show that our new techniques yield the best trade-off between accuracy and efficiency for both local and global silhouette estimation. In addition, our methods scale efficiently to massive datasets for which an exact computation of the silhouette is not practical.

1 Introduction

Clustering is of fundamental importance for data analysis, with ubiquitous applications in various areas including pattern recognition [Xu and Tian, 2015], bioinformatics and biomedicine [Ikotun et al., 2023], and data management [Aggarwal and Reddy, 2014, Karypis and Kumar, 1998]. Broadly, clustering a dataset requires grouping elements with high similarity, and separating dissimilar elements [Kleinberg, 2002]. The clustering of a dataset is often viewed as an optimization problem, where the objective varies according to the desired properties of the optimal clustering. A large number of algorithms have been designed to cluster a dataset according to various objectives [Hennig et al., 2015]. In particular, recent research for clustering methods has its focus on the design of rigorous and scalable approaches to cluster massive datasets [Barger and Feldman, 2016, Ceccarello et al., 2017, 2019, Malkomes et al., 2015, Mazzetto et al., 2019, Pranjali and Balcan, 2013].

The vast number of clustering objectives and methods, introduce the need for rigorous methods to identify “good quality” clusterings of a dataset [Liu et al., 2010, Schubert, 2023]. *Clustering evaluation* (or simply *validation*) assesses the quality of a given clustering relying on an evaluation measure. An evaluation measure is either *external* (i.e., *supervised*) or *internal* (i.e., *unsupervised*). Supervised measures rely on external knowledge about the data, e.g., ground truth labels—rarely available [Tan et al., 2005]. In contrast, internal measures evaluate the quality of a clustering relying uniquely on the dataset. Due to their broad applicability, internal measures are widely used in practice to identify high-quality clusterings [Hassan et al., 2024].

The *silhouette* is one of the most commonly used internal measures for clustering evaluation [Hassan et al., 2024, Rousseeuw, 1987]. The silhouette $s(e)$ of an element e assigned to a cluster C is defined as the ratio $(b(e) - a(e)) / \max\{a(e), b(e)\}$ where $a(e)$ is the average distance of e from the other elements of C , and $b(e)$ is the minimum average distance of e from the elements of a cluster C' different from C . In other words, $s(e)$ provides a simple to interpret score between -1 and 1, which captures the quality of the assignment of e to its group C . That is, if e is closer (on average) to the elements in its cluster C than to the elements in the “closest” cluster $C' \neq C$, then $s(e)$ will be close to 1. In contrast, $s(e)$ becomes negative when the element e is closer to the elements in C' . As an example, consider elements e_{13} and e_{14} in Figure 1a (where the distance is the Euclidean distance): *i*) the silhouette $s(e_{13})$ is positive since e_{13} is closer to the elements of its cluster (e_{11} and e_{12}) compared to its average distance from the elements of other clusters; *ii*) the silhouette $s(e_{14})$ is close to -1 since e_{14} is very close to all elements of cluster C_3 and distant from the other elements of its cluster C_1 . Hence, the silhouette $s(e)$ of an element e (or *local silhouette*) provides an interpretable and reliable score to assess the quality of the assignment of each element e to its cluster [Dinh et al., 2019, Lovmar et al., 2005].

Furthermore, the *average silhouette* of *all* elements, known as the silhouette of a clustering (or *global silhouette*), has a plethora of applications in many important areas [Hossain and Angryk, 2007, Ng and Han, 1994, Sellam et al., 2016, Wiwie et al., 2015], and is described in widely used data mining textbooks [Han et al., 2011, Tan et al., 2005]. As an example, the silhouette of a clustering can be used to identify a good value for the number k of clusters computed by popular clustering algorithms, e.g., k -means, or k -medoids [Dinh et al., 2019, Lenssen and Schubert, 2024].

For general distance metrics, the exact computation of the silhouette for a k -clustering of n

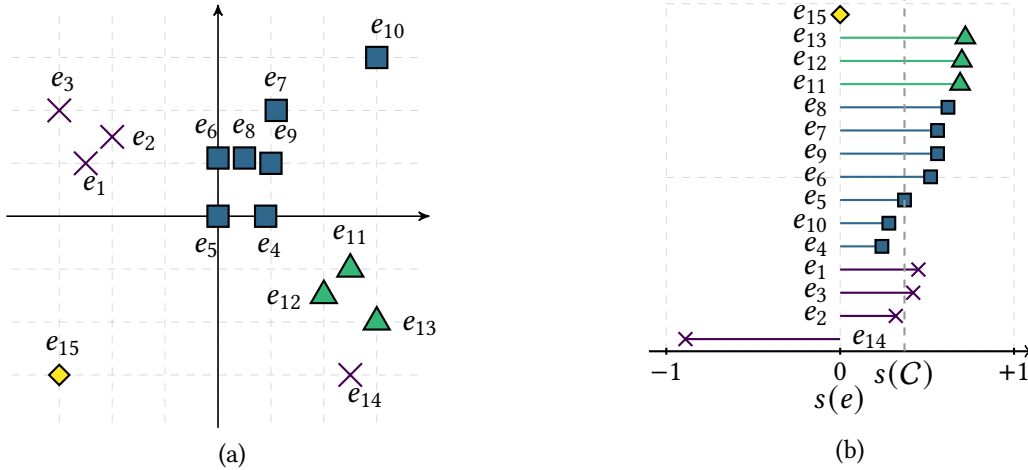


Figure 1: (a): dataset $V = \{e_1 \dots, e_n\}$ for $n = 15$ with elements in the Euclidean plane \mathbb{R}^2 . Different shapes represent $k = 4$ different clusters, that is $C = \{C_1 = \{e_1, \dots, e_3, e_{14}\}, C_2 = \{e_4, \dots, e_{10}\}, C_3 = \{e_{11}, e_{12}, e_{13}\}, C_4 = \{e_{15}\}\}$. (b): silhouette $s(e)$ of the elements $e \in V$ (where the distance is the Euclidean distance): values are grouped by clusters and sorted. The dashed line represents the value of the *silhouette of the clustering* C , marked with $s(C)$. Such representation is known as the *silhouette plot* [Rousseeuw, 1987].

elements requires $\Theta(n^2)$ distance calculations, irrespective of k . The quadratic barrier constitutes a key challenge that prevents silhouette-based analyses on modern massive datasets. Surprisingly, for such a general setting, there are no methods to efficiently approximate the silhouette with *provably high accuracy* guarantees and breaking the $\Theta(n^2)$ barrier. In contrast, various scalable techniques have been proposed to efficiently cluster large datasets with rigorous guarantees, especially in distributed environments [Bahmani et al., 2012, Balcan et al., 2013, Ene et al., 2011, Feldman and Langberg, 2011, Malkomes et al., 2015].

In this work, we introduce the *first randomized approximation algorithms* with rigorous (probabilistic) guarantees on the quality of their estimates for two key problems: *i*) estimating the silhouette of each element e of a given clustering; *ii*) estimating the global silhouette of a clustering. Our algorithms feature a memory-efficient distributed implementation in popular frameworks such as *MapReduce* [Dean and Ghemawat, 2008, Leskovec et al., 2014, Pietracaprina et al., 2012], and the *Massively Parallel Computing* (MPC) model [Im et al., 2023], in analogy with state-of-the-art scalable clustering algorithms. Similar to other randomized algorithms, the guarantees of our methods are controlled by two easy to interpret parameters ϵ and δ , controlling the trade-off between efficiency and accuracy. In particular, ϵ controls the (absolute) error between the output of our methods and the actual values being estimated, and δ controls the error probability (all our results hold with probability at least $1 - \delta$).

For the estimation of the silhouette of each element e , we rely on the Probability Proportional to Sampling (PPS) technique by Chechik et al. [2015], which can be used to obtain highly accurate estimates of the average distance between e and the elements of a given cluster. For a k -clustering, our method performs $\mathcal{O}(nk\epsilon^{-2} \log(nk/\delta))$ distance computations, producing estimates $\widehat{s}(e)$ such that $|s(e) - \widehat{s}(e)| \leq f(\epsilon)$ with $f(\epsilon) = \mathcal{O}(\epsilon)$ with probability at least $1 - \delta$, simultaneously for *all*

elements e . Note the substantial improvement over the $\Theta(n^2)$ distance computations of an exact method, at the expense of a small estimation error.

For the global silhouette estimation, we design three estimators, including a simple algorithm that computes the average silhouette using a small random subset of elements, and two slightly more complex algorithms relying on the PPS approach. We show in our analysis that all our methods perform $o(n^2)$ distance computations, and report an estimate with bounded error from the actual global silhouette, with controlled error probability. Finally, our experiments show that all our methods are extremely efficient and scalable in practice, especially on large datasets, where exact approaches are infeasible and existing techniques perform poorly.

Our contributions. To summarize our contributions are as follows.

- We present the first rigorous sampling-based approximation algorithms for two key problems involving the silhouette: *i*) estimating the silhouette of all elements of a clustered dataset; *ii*) estimating the global silhouette of a clustering. Our methods require the distance between elements to be defined through a metric.
- We prove that all our methods require a significantly smaller number of distance computations than $\Theta(n^2)$, reporting high-quality estimates with (absolute) error controlled by parameter ε , with probability controlled by parameter δ .
- We provide a distributed MapReduce design of our methods and discuss how our methods can be ported to the popular MPC framework. Our distributed methods use sublinear local memory (at each worker) and a constant number of rounds, two features that are highly desirable when processing massive datasets.
- We perform an extensive experimental evaluation on medium- and large-size datasets with multiple goals: *i*) assess the trade-off between the quality of the estimates and the number of distance computations of our methods for estimating the global silhouette of the entire clustering; *ii*) evaluate the accuracy of our method for the estimation of the local silhouette for all elements; *iii*) assess the performance of our distributed methods; *iv*) illustrate applications of our new methods, leveraging both the global and local silhouette.

Contributions over the conference version. A preliminary version of this work was presented at the SIAM International Conference on Data Mining, 2021, authored by a subset of the authors [Altieri et al., 2021]. This work features substantial modifications and additions to that preliminary work, as summarized below.

- We propose two novel estimators for the global silhouette coefficient, in addition to the estimator originally devised in [Altieri et al., 2021]. Our new methods require considerably fewer samples compared with the method appeared in [Altieri et al., 2021], yielding a reduction in the time complexity for global estimation.
- We rigorously study the problem of local silhouette estimation, providing: *i*) a sound algorithm to solve the local silhouette estimation problem, based on techniques appeared in our previous version; *ii*) rigorous bounds on the sample complexity, fixing existing issues with previous proofs in the literature [Chechik et al., 2015]; *iii*) we prove that the

guarantees of our new method based on PPS sampling cannot be matched by a simpler and more intuitive uniform sampling-based approach—supporting the design of our method.

- We include all proofs omitted from [Altieri et al., 2021] for space constraints.
- We show how the distributed MapReduce implementation of our methods can be ported to the popular MPC framework, which is widely adopted for large-scale data analysis.
- We perform a new and extensive experimental evaluation, over medium- and large-size real datasets available online, showing the effectiveness of our approaches in various settings.

The paper is structured as follows. In [Section 2](#), we introduce the necessary preliminary notions. In [Section 3](#), we discuss relevant previous work, with a focus on the silhouette approximation. In [Section 4](#), we introduce our methods and their analysis. In [Section 5](#), we present the results of our extensive experimental evaluation. Lastly, [Section 6](#) summarizes our concluding remarks.

The code and necessary material to reproduce our results is available at the following repository <https://github.com/iliesarpe/ScalableSilhouetteComputation>.

2 Preliminaries

Let U be a metric space equipped with a distance function $d(\cdot, \cdot)$, and let $V = \{e_1, \dots, e_n\} \subseteq U$ be a dataset of n distinct elements from U . Let $C = \{C_1, \dots, C_k\}$ be a k -clustering¹ of V , that is C consist of a *partition* of V into k disjoint and non-empty subsets called *clusters*. Formally, the *silhouette* $s(e)$ of an element $e \in V$ belonging to a cluster $C \in C$, as introduced by Rousseeuw [1987] is defined as,

$$s(e) \doteq \frac{b(e) - a(e)}{\max\{a(e), b(e)\}} \quad (1)$$

where

$$a(e) = \frac{\sum_{e' \in C} d(e, e')}{|C| - 1}, \quad b(e) = \min_{\substack{C_j \in C, \\ C_j \neq C}} \frac{\sum_{e' \in C_j} d(e, e')}{|C_j|}. \quad (2)$$

That is, $a(e)$ is the average distance of element $e \in V$ from all other elements of its cluster C ; while $b(e)$ is the minimum average distance of $e \in C$ from the elements in some cluster $C_j \in C$ different from C . Note that by [Equation \(1\)](#) it holds that $s(e) \in [-1, 1] \subseteq \mathbb{R}$. If element e is the only element in its cluster C such that $C = \{e\}$, we define $s(e) = 0$, as proposed by Rousseeuw [1987]. As an example, consider e_{15} in [Figure 1](#), then $s(e_{15}) = 0$.

The silhouette $s(e)$ of an element $e \in E$ is a *local measure* that evaluates the quality of a clustering C with respect to the assignment of e to its cluster C . Under a good assignment, the average distance of e to the points in C is much smaller than the average distance to the points of a different cluster, thus from [Equation \(1\)](#) it holds $s(e) \approx 1$. Hence, high-values of $s(e)$ denote a “good” assignment of element e to its cluster C . Conversely, if e is, on average, much

¹We will drop k when clear from the context.

closer to the elements of a different cluster $C_j \neq C$ then by Equation (1) it holds $s(e) \approx -1$, i.e., a “bad” cluster assignment for e . The individual $s(e)$ ’s are often represented through the *silhouette plot* [Rousseeuw, 1987], where the abscissae range in $[-1, 1]$ (possible silhouette values) and the ordinate values correspond to the distinct elements, ordered by clusters.

Example 1. Consider the dataset from Figure 1a and $d(\cdot, \cdot)$ being the Euclidean distance.² Figure 1b shows its silhouette plot, with points grouped by cluster. We observe that, for $e_{11} \in C_3$ it holds $s(e_{11}) > 0$ since e_{11} is much closer to e_{12} and e_{13} than to the points of any other cluster different from C_3 . In contrast, consider e_{14} , then $b(e_{14}) = (d(e_{11}, e_{14}) + d(e_{12}, e_{14}) + d(e_{13}, e_{14}))/3 < (d(e_1, e_{14}) + d(e_2, e_{14}) + d(e_3, e_{14}))/3 = a(e_{14})$. Therefore $s(e_{14}) < 0$, capturing the intuition that assigning e_{14} to C_3 instead of C_1 leads to a better clustering.

The *silhouette of a clustering C* evaluates the quality of a clustering C as the *average silhouette* of all the elements $e \in V$. Formally, the silhouette $s(C)$ of a clustering C is

$$s(C) \doteq \frac{1}{n} \sum_{i=1}^n s(e_i) . \quad (3)$$

Therefore, $s(C)$ provides a *global measure* of the quality of the whole clustering C , where a value close to 1 denotes a high quality of the clustering C .

Example 2. Consider Figure 1b under the setting of Example 1: we observe that for the global silhouette of the clustering C it holds $s(C) \approx 0.36$. That is, on average, most points are well assigned over C , as we can observe from Figure 1a. Clearly, a positive value for $s(C)$, does not imply that all points have $s(e) > 0$, e.g., $s(e_{14}) < 0$.

In practice, the score $s(C)$ is widely used to identify a good value for k (e.g., [Lleti et al., 2004]). That is, analysts often compare various clusterings $\{C_{k_i}\}_{i \geq 1}$ obtained with different values of k_i , selecting the best value of k as the one maximizing $s(C_{k_i})$, for $i \geq 1$. In fact, using the silhouette to select a good value of k for a k -clustering is highly effective and reliable, in contrast to other popular methods, such as the elbow method, which often lead to poor results [Schubert, 2023].

It is clear from Equation (1) that the straightforward computation of $s(e)$ for each element $e \in V$ and the subsequent computation of $s(C)$ require $\Theta(n^2)$ distance calculations. We remark that such a quadratic complexity is *extremely resource demanding* even when dealing with medium-sized datasets, i.e., impractical for modern massive data volumes.

Finally, we wish to recall that for an algorithm employing random sampling, its *sample complexity* refers to the total number of samples generated throughout its execution [Mitzenmacher and Upfal, 2017].

3 Related work

Since the introduction of the silhouette metric by Rousseeuw [1987], its use has been ubiquitous for clustering applications [Arbelaitz et al., 2013, Moulavi et al., 2014, Tomasini et al., 2016, Xiong

²Recall for $\mathbf{x}, \mathbf{y} \in \mathbb{R}^z$ the Euclidean distance $d(\mathbf{x}, \mathbf{y})$ is $\sqrt{\sum_i (x_i - y_i)^2}$ where $x_i, i \in [z]$ denotes the i -th coordinate of \mathbf{x} .

and Li, 2013], including the use of the silhouette to obtain new clustering objectives for both k -medoids [Kaufmann and Rousseeuw, 1987, Lenssen and Schubert, 2024] and k -means [Lai et al., 2024]. However, as observed before, obtaining the exact silhouette is impractical for large datasets, due to the $\Theta(n^2)$ distance computations required. Therefore, various methods have been proposed to reduce the time complexity, or to simplify the silhouette calculation under certain assumptions. In this section, we review to the most relevant methods for silhouette approximation, which mostly apply to center-based clusterings. That is, clusterings where each cluster is associated with a distinguished center from the metric space (e.g., the centroids in the case of k -means clusterings).

Van der Laan et al. [2003] introduced a variant of the silhouette $s(e)$, where the term $b(e)$ is computed as the distance from the closest center, other than the cluster e belongs to (while $a(e)$ is computed according to Equation (2)). Following such idea, Hruschka et al. introduced the *simplified silhouette*. The simplified silhouette for an element e assigned to cluster C evaluates $a(e)$ as the distance between e and the center of C , and $b(e)$ as the distance between e and the closest center of a cluster different from C . The complexity of computing the simplified silhouette reduces to $\mathcal{O}(nk)$. Hruschka et al. and Wang et al. [2017] show empirically that the simplified silhouette can be an effective evaluation measure for clusterings returned by Lloyd’s algorithm [Lloyd, 1982]. However, there is no evidence of the effectiveness of the simplified silhouette for other clusterings (e.g. based on arbitrary distance functions). In addition, as shown in our experimental evaluation in Section 5, the difference between the values of the silhouette (Equation (1)) and the simplified silhouette, can be arbitrary large, making the simplified silhouette unreliable for rigorous silhouette-based analyses.

A different heuristic for improving the computation of the exact silhouette of center-based clusterings under Euclidean distances was introduced by Frahling and Sohler [2008]. For each element e of a cluster C , the term $a(e)$ is computed according to its definition (Equation (2)), while for $b(e)$ the heuristic first determines the average distance $\bar{d}_{e,C'}$ between e and the elements of the cluster $C' \neq C$, whose centroid is closest to e . If, for any other cluster $C'' \notin \{C, C'\}$, it holds that the distance between e and the centroid of C'' is greater than or equal to $\bar{d}_{e,C'}$, then it sets $b(e) = \bar{d}_{e,C'}$, otherwise it computes $b(e)$ according to Equation (2). For Euclidean distances, it can be shown that in the former case $\bar{d}_{e,C'}$ coincides exactly with the value of $b(e)$ defined in Equation (2). The worst case complexity remains quadratic, but the heuristic likely performs less than $\Theta(n^2)$ distance computations in practice.

The Apache Spark programming framework provides optimized methods for computing the silhouette of a clustering under d -dimensional *squared Euclidean* distances and under one formulation of cosine distance.³ For such specific distances, simple algebra suffices to show that the pre-computation of a limited number of values dependent on the coordinates of the points in each of the k clusters yields a parallelizable algorithm performing $\mathcal{O}(nkd)$ distance computations. However, the above optimization does not apply to *arbitrary* distance metrics, as of interest in our work.

The methods presented in this paper apply to any metric distance and provide provably accurate silhouette estimations. Our methods rely on the use a *Probability Proportional to Size* (PPS) sampling scheme, where each element is sampled with a probability proportional to a certain “size” measure. The use of PPS sampling has been pioneered in the context of center-based

³<https://spark.apache.org/>

clustering algorithms, distance query processing and centrality estimation in graphs [Balcan et al., 2013, Chechik et al., 2015, Cohen et al., 2018, Feldman and Langberg, 2011]. To the best of our knowledge, prior to the conference version of the current work [Altieri et al., 2021] the use of PPS for efficient clustering evaluation had not been explored.

4 Methods

In this section we present our methods. In [Section 4.1](#) we focus on the estimation of the silhouette of all individual elements, while in [Section 4.2](#) we focus on the estimation of the silhouette of the whole clustering. Finally, [Section 4.3](#) describes scalable distributed implementations of our methods on the MapReduce and MPC frameworks.

4.1 Estimating the silhouette of each element

In this section we address the following problem,

Problem 1. *Given a dataset V from an arbitrary metric space, a k -clustering C , and two parameters $\varepsilon, \delta \in (0, 1)$, obtain $\widehat{s}(V) = \{(e, \widehat{s}(e)) : e \in V\}$ such that, with probability at least $1 - \delta$, $|\widehat{s}(e) - s(e)| = O(\varepsilon)$ simultaneously for each element $e \in V$, minimizing the number of distance computations performed.*

Our main result, addressing [Problem 1](#) is the following.

Theorem 1. *Consider a dataset V , a k -clustering C , and two parameters $\varepsilon, \delta \in (0, 1)$. There exists a randomized algorithm based on PPS sampling with sample complexity $O(k\varepsilon^{-2} \log(nk/\delta))$ that, with probability $1 - \delta$:*

1. *returns a set $\widehat{s}(V) = \{(e, \widehat{s}(e)) : e \in V\}$ such that, for all $e \in V$, $|\widehat{s}(e) - s(e)| \leq 4\varepsilon/(1 - \varepsilon)$;*
2. *performs $O(nk\varepsilon^{-2} \log(nk/\delta))$ distance computations.*

[Theorem 1](#) shows that we can obtain a very accurate probabilistic approximation of each silhouette value $s(e), e \in V$. For practical values of $k \ll n$, and constant ε and δ , the result of [Theorem 1](#) breaks the quadratic barrier of $\Theta(n^2)$ distance computations, enabling the efficient and practical computation of silhouette values over large and massive datasets. Note that the $O(\varepsilon^{-2})$ factor in the sample complexity and in the number of distance computations from [Theorem 1](#), might become large for small ε . While a quadratic dependence on ε cannot be avoided in a worst-case analysis [Mitzenmacher and Upfal, 2017], in practice, even large values of ε (e.g., close to 1) yield highly accurate estimates for *all* values in $\widehat{s}(V)$.

In this section, we also provide evidence that PPS is crucial to achieve our result. Namely, we argue that, under the same sample complexity of [Theorem 1](#), a more intuitive *uniform sampling* approach performs arbitrarily poorly.

Theorem 2. *There exists a large dataset V , and a 2-clustering C of V , such that the same algorithm as the one of [Theorem 1](#), modified replacing PPS sampling with uniform sampling, returns a set of estimates $\widehat{s}(V) = \{(e, \widehat{s}(e)) : e \in V\}$, with arbitrarily large probability, such that: $|\widehat{s}(e') - s(e')| \geq 1$ for at least $n/2 - 1$ elements $e' \in V$.*

[Theorem 2](#) indicates that uniform sampling cannot guarantee an (arbitrarily small) estimation error $O(\varepsilon)$ using a sublinear sample size, in contrast with [Theorem 1](#).

In the rest of this section, we describe our main algorithm ([Section 4.1.1](#)) and prove the above two key results (in [Sections 4.1.2](#) and [4.1.3](#), respectively).

4.1.1 Algorithm

Consider the setting of [Problem 1](#). For each element $e \in V$ and cluster $C_j \in \mathcal{C}$, let

$$W_{C_j}(e) = \sum_{e' \in C_j} d(e, e') . \quad (4)$$

Given the definition of $W_{C_j}(e)$ in [Equation \(4\)](#), for an element e of a cluster C we can express the quantities $a(e)$ and $b(e)$ in the definition of the silhouette $s(e)$ (from [Equation \(2\)](#)) as

$$a(e) = \frac{W_C(e)}{|C| - 1} \quad \text{and} \quad b(e) = \min_{C_j \neq C} \frac{W_{C_j}(e)}{|C_j|} .$$

Building on the above formulation, we rely on the accurate estimation of the terms $W_{C_j}(e)$ to approximate the silhouette $s(e)$ for each element $e \in V$.

A first attempt to obtain an estimate of $W_{C_j}(e)$ would be to sample *uniformly* at random a set of $t \geq 1$ points from each cluster $C_j \in \mathcal{C}$ to be used to estimate $W_{C_j}(e)$. Unfortunately, in [Section 4.1.3](#) we show an instance of V and \mathcal{C} where such an approach fails with large probability for the sample complexity guarantees of [Theorem 1](#) over a large fraction of points (see [Theorem 2](#)). That is, with a uniform sampling approach we *cannot* obtain the accurate approximation of the silhouette values as captured in [Problem 1](#) with the guarantees provided by [Theorem 1](#).

Therefore, to achieve an accurate estimation of the weights $W_{C_j}(e)$, we exploit the more complex but effective *Probability Proportional to Size* (PPS) sampling strategy proposed by [Chechik et al. \[2015\]](#). The PPS sampling strategy allows us to collect a suitable *small* sample F_{C_j} from each cluster C_j . The sample F_{C_j} can be then used to approximate the value of $W_{C_j}(e)$ of every element $e \in V$, within user-defined error bounds and with high probability, using only *weighted* distances between e and elements in F_{C_j} . The selection of the elements of F_{C_j} is *not* uniformly at random. Instead, it involves carefully designed sampling probabilities that favor the selection of distant elements from a suitable “central” element of each cluster C_j for $j \in [k]$.

At high level, our algorithm SILH-PPS-ALL ([Algorithm 1](#)), consists of two *phases*: 1) For each cluster $C_j \in \mathcal{C}$, the algorithm computes a sample F_{C_j} of *expected* size $t = \lceil (c\varepsilon^{-2}) \ln(5nk/\delta) \rceil$ for a suitably small constant c ; 2) each sample F_{C_j} is then used to estimate the weights $W_{C_j}(e)$ for $j \in [k]$, and such weights are combined to obtain $\hat{s}(e)$, i.e., the estimates of $s(e)$ for each $e \in V$. More in detail.

Phase 1. Each cluster $C_j, j \in [k]$ is processed independently. If $|C_j| \leq t$, then F_{C_j} is set to C_j . Otherwise, we perform *Poisson sampling* over C_j where each element $e \in C_j$ is included in F_{C_j} independently with a suitable probability p_e . For $e \in C_j$, probability p_e is determined as follows:

Algorithm 1: SILH-PPS-ALL

Input: Clustering $C = \{C_1, \dots, C_k\}$ of $V = \{e_1, \dots, e_n\}$ and $\varepsilon, \delta \in (0, 1), t \geq 2$.

Output: $\hat{s}(V) = \{(e_1, \hat{s}(e_1)), \dots, (e_n, \hat{s}(e_n))\}$.

▷ Phase 1: *PPS sampling*

```
1  $n \leftarrow |V|; t \leftarrow \lceil (ce^{-2}) \ln(5nk/\delta) \rceil;$ 
2 for each cluster  $C_j \in C$  do
3   if  $|C_j| \leq t$  then  $F_{C_j} \leftarrow C_j;$ 
4   else
5      $F_{C_j}^0 \leftarrow$  Poisson sampling of  $C_j$  with probability  $(2/|C_j|) \ln(5k/\delta);$ 
6     for each  $\bar{e} \in F_{C_j}^0$  do  $W_{C_j}(\bar{e}) \leftarrow \sum_{e' \in C_j} d(\bar{e}, e');$ 
7     for each  $e \in C_j$  do
8        $\gamma_e \leftarrow \max\{d(e, \bar{e})/W_{C_j}(\bar{e}) : \bar{e} \in F_{C_j}^0\};$ 
9        $\gamma_e \leftarrow \max\{1/|C_j|, \gamma_e\};$ 
10       $p_e \leftarrow \min\{1, t\gamma_e\};$ 
11       $F_{C_j} \leftarrow$  Poisson sampling of  $C_j$  with probabilities  $\{p_e : e \in C_j\};$ 
```

▷ Phase 2: *Silhouette estimation*

```
12 for each  $e \in V$  do
13   Let  $e$  belong to cluster  $C;$ 
14   for each cluster  $C_j$  do
15      $\widehat{W}_{C_j}(e) = \sum_{e' \in F_{C_j}} d(e, e')/p_{e'};$ 
16      $\widehat{a}(e) \leftarrow \widehat{W}_C(e)/(|C| - 1);$ 
17      $\widehat{b}(e) \leftarrow \min\{\widehat{W}_{C_j}(e)/|C_j| : C_j \neq C\};$ 
18      $\widehat{s}(e) \leftarrow (\widehat{b}(e) - \widehat{a}(e))/(\max\{\widehat{a}(e), \widehat{b}(e)\});$ 
19 return  $\widehat{s}(V) = \{(e, \widehat{s}(e)) : e \in V\};$ 
```

- First, we select an initial sample $F_{C_j}^0$, by Poisson sampling. That is, each $e \in C_j$ is included in $F_{C_j}^0$ independently with fixed probability $(2/|C_j|) \ln(5k/\delta)$. Each sample $F_{C_j}^0$ will contain, with sufficiently high probability, an aforementioned “central” element of C_j .⁴
- We then compute the value $W_{C_j}(\bar{e})$ for each sampled element $\bar{e} \in F_{C_j}^0$. Then, for each $e \in C_j$ we set $p_e = \min\{1, t\gamma_e\}$, where γ_e is computed as

$$\gamma_e = \max \left\{ \underbrace{\frac{1}{|C_j|}}_{T_1}, \underbrace{\max_{\bar{e} \in F_{C_j}^0} \frac{d(e, \bar{e})}{W_{C_j}(\bar{e})}}_{T_2} \right\}.$$

⁴A *central* element, is an element close to a majority of the elements of C_j , see the proof of [Lemma 1](#) for a formal definition.

For $e \in C_j$, γ_e is the maximum between two terms T_1 and T_2 . Where, T_1 corresponds to the probability of selecting e uniformly among all elements of C_j , ensuring that all points have a sufficiently large probability of being sampled; while T_2 corresponds to the maximum relative contribution of e to the weights $W_{C_j}(\bar{e})$ of elements $\bar{e} \in F_{C_j}^0$. The intuition is that a higher relative contribution of element $e \in C_j$ to $W_{C_j}(\bar{e})$ implies that element $e \in C_j$ is extremely important for the accurate estimation of $W_{C_j}(\bar{e})$ with $\bar{e} \in F_{C_j}^0$ —captured by the value γ_e through T_2 , which yields a high sampling probability p_e for $e \in C_j$.

Phase 2. We now have access to a sample F_{C_j} obtained through Poisson sampling with individual probabilities p_e for each $e \in V$ (computed over **Phase 1**), over each cluster C_j . Hence, we use each F_{C_j} to obtain the estimates

$$\widehat{W}_{C_j}(e) = \sum_{e' \in F_{C_j}} \frac{d(e, e')}{p_{e'}} ,$$

which are accurate estimators of $W_{C_j}(e)$, as we prove in our analysis (Section 4.1.2). We then use values $\widehat{W}_{C_j}(e)$, $j \in [k]$, $e \in V$ to compute $\widehat{s}(e)$, $e \in V$ as follows. Let $e \in V$ with $e \in C$, $C \in \mathcal{C}$, we compute estimates $\widehat{a}(e) = \frac{\widehat{W}_C(e)}{(|C|-1)}$ and $\widehat{b}(e) = \min_{C_j \neq C} \left\{ \frac{\widehat{W}_{C_j}(e)}{|C_j|} \right\}$. Finally we obtain the estimates $\widehat{s}(e)$ of the silhouette of each element $e \in V$ as

$$\widehat{s}(e) = \frac{\widehat{b}(e) - \widehat{a}(e)}{\max \{ \widehat{a}(e), \widehat{b}(e) \}} . \quad (5)$$

Algorithm 1 (SILH-PPS-ALL) reports all details of the resulting procedure that combines the phases described above.

4.1.2 Proof of Theorem 1

We prove **Theorem 1** in two steps. First, we show that, with probability at least $1 - 3\delta/5$, for each element $e \in V$ the value $\widehat{s}(e)$ computed by SILH-PPS-ALL approximates the actual value $s(e)$ within a small absolute error expressed as a function $f(\varepsilon) = \Theta(\varepsilon)$, with $\varepsilon \in (0, 1)$. Second, we upper bound the sample complexity and the number of distance computations with probability at least $1 - 2\delta/5$.

Our key ingredient is the next lemma that provides a probabilistic upper bound on the *relative* approximation error of the estimates $\widehat{W}_{C_j}(e)$ with respect to the actual values $W_{C_j}(e)$ for an arbitrary element $e \in V$, and $j \in [k]$.

Lemma 1. *Let $c = 18$. If $t = \lceil (3c/\varepsilon^2) \ln(5nk/\delta) \rceil$, then with probability at least $1 - 3\delta/5$, for every element $e \in V$ and every cluster C_j , the estimate $\widehat{W}_{C_j}(e)$ computed by SILH-PPS-ALL is such that*

$$\left| \frac{\widehat{W}_{C_j}(e) - W_{C_j}(e)}{W_{C_j}(e)} \right| \leq \varepsilon .$$

Proof. Our proof expands the poorly sketched argument in the proof of [Chechik et al., 2015, Lemma 12]. Consider an arbitrary cluster C_j . If $|C_j| \leq t$ the statement follows trivially, since $\widehat{W}_{C_j}(e) = W_{C_j}(e)$. Thus, we focus on the case $|C_j| > t$. For an element $e \in C_j$, let $m(e)$ denote the median of the distances from e to all other elements of C_j , that is, the distance between e and the $\lceil |C_j|/2 + 1 \rceil$ -th closest element to e in C_j . Let $e_{\min} = \arg \min_{e' \in C_j} m(e')$. The element e is called *well positioned* if $m(e) \leq 2m(e_{\min})$. Using the triangle inequality, it is easy to see that the $\lceil |C_j|/2 \rceil$ elements of C_j closest to e_{\min} are well positioned. Hence, the initial random sample $F_{C_j}^0$ will contain a well positioned element with probability at least

$$1 - \left(1 - \frac{2}{|C_j|} \ln \left(\frac{5k}{\delta}\right)\right)^{\frac{|C_j|}{2}} \geq 1 - \frac{\delta}{5k} ,$$

since $(1 + q/x)^x \leq \exp(q)$, for $x \geq 1$, $|q| \leq x$, and $|C_j|/2 > t/2 > \ln(5k/\delta)$. As proved in Chechik et al. [2015, Lemma 9], if $F_{C_j}^0$ contains a well positioned element, then for $c = 18$ we have that for all $e \in C_j$, the values γ_e computed by Algorithm 1 satisfy

$$\gamma_e \geq \frac{1}{c} \max_{e' \in C_j} \frac{d(e, e')}{W_{C_j}(e')} . \quad (6)$$

To obtain a worst-case bound, we assume that for each $e \in C_j$ it holds that $p_e = t\gamma_e$ where $p_e \leq 1$. In fact, when it holds $p_e = 1$, the contribution of element e to the weights $\widehat{W}_{C_j}(e')$ of all elements $e' \in V$ is always computed *exactly*, implying no error over the estimates $\widehat{W}_{C_j}(e')$. From Equation (6), we have that $p_e \geq (t/c) \max_{e' \in C_j} (d(e, e')/W_{C_j}(e'))$. Fix an arbitrary element $e \in C_j$, and for every $e' \in C_j$ let $X_e(e')$ be the random variable taking value $d(e, e')/p_{e'}$, with probability $p_{e'}$, and 0 otherwise. We have that

$$\widehat{W}_{C_j}(e) = \sum_{e' \in C_j} X_e(e') .$$

It is immediate to see that $\mathbb{E}[\widehat{W}_{C_j}(e)] = W_{C_j}(e)$ by the linearity of expectation and the definition of variables $X_e(e')$. Let $\tau_e = W_{C_j}(e)/(t/c)$ and, for every $e' \in C_j$, let $Y_e(e') = X_e(e')/\tau_e$ be a normalized variable associated to each $X_e(e')$. Note that $Y_e(e') \leq (d(e, e')/W_{C_j}(e))/(\max_{e'' \in C_j} \{d(e'', e')/W_{C_j}(e'')\}) \leq 1$ and therefore $Y_e(e') \in [0, 1]$, hence

$$\mu_e \doteq \mathbb{E} \left[\sum_{e' \in C_j} Y_e(e') \right] = \frac{W_{C_j}(e)}{\tau_e} = \frac{t}{c} .$$

The above discussion implies that

$$\mathbb{P} \left(\widehat{W}_{C_j}(e) \leq (1 + \varepsilon)W_{C_j}(e) \right) = \mathbb{P} \left(\sum_{e' \in C_j} Y_e(e') \leq (1 + \varepsilon) \frac{t}{c} \right) = \mathbb{P} \left(\sum_{e' \in C_j} Y_e(e') \leq (1 + \varepsilon)\mu_e \right) .$$

Since variables $Y_e(e')$'s are independent random variables, and each $Y_e(e')$ takes either value $(1/\tau_e)d(e, e')/p_{e'} \leq 1$ with probability $p_{e'}$, or 0 otherwise, by the application of Theorem 7 (see

Section A) we conclude that

$$\mathbb{P}\left(\sum_{e' \in C_j} Y_e(e') \geq (1 + \varepsilon)\mu_e\right) \leq \exp\left(-\frac{\varepsilon^2 t}{3c}\right) \leq \frac{\delta}{5nk},$$

where the last inequality follows from the choice of t as from the statement. Therefore, we have that

$$\mathbb{P}\left(\widehat{W}_{C_j}(e) \leq (1 + \varepsilon)W_{C_j}(e)\right) \geq 1 - \frac{\delta}{5nk}.$$

A symmetrical argument can be used to also show that

$$\mathbb{P}\left(\widehat{W}_{C_j}(e) \geq (1 - \varepsilon)W_{C_j}(e)\right) \geq 1 - \frac{\delta}{5nk}.$$

By the union bound, the probability that there exists a cluster C_j such that the initial sample $F_{C_j}^0$ does *not* contain a well positioned element is bounded by $k\delta/(5k) = \delta/5$. Now, by conditioning on the event that for all clusters C_j for $j \in [k]$ the initial sample $F_{C_j}^0$ contains a well positioned element, we proceed with a second application of the union bound to prove our claim. That is, the probability that there exists an element $e \in V$ and a cluster C_j for which $|(\widehat{W}_{C_j}(e) - W_{C_j}(e))/W_{C_j}(e)| > \varepsilon$ is at most $2nk\delta/(5nk) = 2\delta/5$. Therefore, the probability that $|(\widehat{W}_{C_j}(e) - W_{C_j}(e))/W_{C_j}(e)| \leq \varepsilon$ for every $e \in V$ is at least $1 - \delta/5 - 2\delta/5 = 1 - 3\delta/5$, yielding the statement and concluding the proof. \square

Let E be the event “the relative error guarantees stated in Lemma 1 hold for every element $e \in V$ and every cluster C_j ”. From now on our analysis conditions on the realization of event E , even when not explicitly stated. Consider an arbitrary element $e \in V$, and let $\widehat{s}(e)$ be the estimate of the silhouette $s(e)$ computed by SILH-PPS-ALL. The following key technical lemma, establishes a bound on the absolute error of the estimates for each element $e \in V$. That is, we show $|\widehat{s}(e) - s(e)| \leq f(\varepsilon)$ as follows.

Lemma 2. *Under event E , SILH-PPS-ALL outputs estimates $\widehat{s}(e)$ for each element $e \in V$ such that,*

$$|\widehat{s}(e) - s(e)| \leq \frac{4\varepsilon}{1 - \varepsilon}.$$

Proof. First note that if $a(e) = 0$ (that is, $\{e\}$ is a singleton cluster), then it follows that $\widehat{a}(e) = 0$ and $s(e) = \widehat{s}(e) = 0$, and the claim trivially holds. We thus consider the case $a(e) > 0$ (also, observe that $b(e) > 0$ by definition). When event E holds, the relative errors of terms: (I) $|(\widehat{a}(e) - a(e))/a(e)|$; and (II) $|(\widehat{b}(e) - b(e))/b(e)|$, are both upper bounded by $\varepsilon > 0$. That is, the bound on term (I) follows immediately from the definition of $\widehat{a}(e)$ and the relative error bound for $\widehat{W}_{C_j}(e)$ provided by Lemma 1. Concerning the bound on the error of term (II), consider an arbitrary cluster C_j and let $b_{C_j}(e) = W_{C_j}(e)/|C_j|$ and $\widehat{b}_{C_j}(e) = \widehat{W}_{C_j}(e)/|C_j|$. Similar to the argument for term (I), it is easy to show that $|(\widehat{b}_{C_j}(e) - b_{C_j}(e))/b_{C_j}(e)| \leq \varepsilon$. Recall that $b(e) = \min_{C_j \neq C} b_{C_j}(e)$ and that $\widehat{b}(e) = \min_{C_j \neq C} \widehat{b}_{C_j}(e)$. Suppose that $b(e) = b_{C'}(e)$ and $\widehat{b}(e) = \widehat{b}_{C''}(e)$, for some, possibly different, clusters C' and C'' . We have:

$$(1 - \varepsilon)b(e) = (1 - \varepsilon)b_{C'}(e) \leq (1 - \varepsilon)b_{C''}(e) \leq \widehat{b}_{C''}(e) = \widehat{b}(e)$$

and

$$\widehat{b}(e) = \widehat{b}_{C'}(e) \leq \widehat{b}_{C'}(e) \leq (1 + \varepsilon)b_{C'}(e) = (1 + \varepsilon)b(e) ,$$

and the desired bound follows.

Now we establish a bound on the relative error for the the denominator of the estimator $\widehat{s}(e)$ (see [Equation \(5\)](#)). Define $M(e) \doteq \max\{a(e), b(e)\}$ and $\widehat{M}(e) \doteq \max\{\widehat{a}(e), \widehat{b}(e)\}$. We show that $|(\widehat{M}(e) - M(e))/M(e)| \leq \varepsilon$. Suppose that $M(e) = a(e)$, hence $a(e) \geq b(e)$ (the case $M(e) = b(e)$ is analogous). If $\widehat{M}(e) = \widehat{a}(e)$, the bound is immediate. Instead, if $\widehat{M}(e) = \widehat{b}(e)$, hence $\widehat{b}(e) \geq \widehat{a}(e)$, the bound follows since

$$\widehat{M}(e) = \widehat{b}(e) \leq (1 + \varepsilon)b(e) \leq (1 + \varepsilon)a(e) = (1 + \varepsilon)M(e) ,$$

and

$$\widehat{M}(e) = \widehat{b}(e) \geq \widehat{a}(e) \geq (1 - \varepsilon)a(e) = (1 - \varepsilon)M(e) .$$

We are now ready to obtain a bound on the absolute difference $|\widehat{s}(e) - s(e)|$. Using the relative error bounds established above, we have that

$$\widehat{s}(e) = \frac{\widehat{b}(e) - \widehat{a}(e)}{\widehat{M}(e)} \leq \frac{(1 + \varepsilon)b(e) - (1 - \varepsilon)a(e)}{(1 - \varepsilon)M(e)} = \frac{(1 + \varepsilon)b(e) - (1 - \varepsilon)a(e)}{(1 - \varepsilon)a(e)} .$$

Simple algebraic manipulations show that

$$\frac{(1 + \varepsilon)b(e) - (1 - \varepsilon)a(e)}{(1 - \varepsilon)a(e)} = s(e) + \frac{2\varepsilon}{1 - \varepsilon} (s(e) + 1) \leq s(e) + \frac{4\varepsilon}{1 - \varepsilon} ,$$

where the last inequality follows since $s(e) \leq 1$. With analogous calculations, we obtain that

$$\begin{aligned} \widehat{s}(e) &= \frac{\widehat{b}(e) - \widehat{a}(e)}{\widehat{M}(e)} \geq \frac{(1 - \varepsilon)b(e) - (1 + \varepsilon)a(e)}{(1 + \varepsilon)M(e)} = \frac{(1 - \varepsilon)b(e) - (1 + \varepsilon)a(e)}{(1 + \varepsilon)a(e)} \\ &= s(e) - \frac{2\varepsilon}{1 + \varepsilon} (s(e) + 1) \geq s(e) - \frac{4\varepsilon}{1 + \varepsilon} \geq s(e) - \frac{4\varepsilon}{1 - \varepsilon} , \end{aligned}$$

which concludes the proof. \square

We observe that [Lemma 2](#) provides rigorous probabilistic guarantees (holding with probability at least $1 - 3\delta/5$) on the approximation error of each element in the set $\widehat{s}(V)$ returned by SILH-PPS-ALL, holding simultaneously for all the elements in V . Note that, for example, when $\varepsilon \leq 1/2$ then $4\varepsilon/(1 - \varepsilon) \leq 8\varepsilon = \mathcal{O}(\varepsilon)$.

To complete the proof of [Theorem 1](#), we now bound the sample complexity and the number of distance computations performed by [Algorithm 1](#), as follows.

Lemma 3. *With probability at least $1 - 2\delta/5$, over the execution of SILH-PPS-ALL, for every cluster C_j with $|C_j| > t$ it holds that,*

$$|F_{C_j}^0| = \mathcal{O}\left(\ln\left(\frac{k}{\delta}\right)\right) \quad \text{and} \quad |F_{C_j}| = \mathcal{O}\left(\varepsilon^{-2} \ln\left(\frac{nk}{\delta}\right)\right) .$$

Proof. Consider a cluster $|C_j|$ with $|C_j| > t$. $|F_{C_j}^0|$ corresponds to a binomial random variable $\text{Bin}(|C_j|, 2/|C_j| \ln(5k/\delta))$, implying that $\mathbb{E}[|F_{C_j}^0|] = 2 \ln(5k/\delta)$. Therefore, a simple application of the Chernoff bound suffices to show that $|F_{C_j}^0| = O(\ln(k/\delta))$ with probability at least $1 - \delta/(5k)$, hence the bound holds for all $F_{C_j}^0$'s with probability at least $1 - \delta/5$. Let us now bound the size of $|F_{C_j}|$ (our result expands on the argument of Chechik et al. [2015]). $|F_{C_j}|$ is a Poisson binomial random variable with expectation

$$\mathbb{E}[|F_{C_j}|] = \sum_{e \in C_j} p_e \leq t \sum_{e \in C_j} \gamma_e .$$

Observe that

$$\begin{aligned} \sum_{e \in C_j} \gamma_e &= \sum_{e \in C_j} \max \left\{ \frac{1}{|C_j|}, \max_{\bar{e} \in F_{C_j}^0} \frac{d(e, \bar{e})}{W_{C_j}(\bar{e})} \right\} && \text{(by definition of } \gamma_e, e \in V) \\ &\leq 1 + \sum_{e \in C_j} \max_{\bar{e} \in F_{C_j}^0} \frac{d(e, \bar{e})}{W_{C_j}(\bar{e})} && \text{(for } A, B \geq 0 \text{ then } \max\{A, B\} \leq A + B) \\ &\leq 1 + \sum_{e \in C_j} \sum_{\bar{e} \in F_{C_j}^0} \frac{d(e, \bar{e})}{W_{C_j}(\bar{e})} && \text{(max}\{A_i\} \leq \sum A_i, A_i \geq 0) \\ &= 1 + \sum_{\bar{e} \in F_{C_j}^0} \sum_{e \in C_j} \frac{d(e, \bar{e})}{W_{C_j}(\bar{e})} && \text{(swapping finite and bounded sums)} \\ &= 1 + |F_{C_j}^0| && \text{(definition of } W_{C_j}(\bar{e})) . \end{aligned}$$

Now consider the following cases: (I) $|F_{C_j}^0| = 1$ consists of a *single well-positioned element*; (II) $|F_{C_j}^0| = |C_j|$, i.e., the initial sample size consists of *all* elements of C_j ; (III) $1 < |F_{C_j}^0| < |C_j|$, accounting for the remaining cases. Clearly, by the above analysis, case (I) yields $\sum_e \gamma_e \leq 2$. Now let us define $\bar{\gamma}_e = \max\{1/|C_j|, \max_{e' \in C_j} d(e, e')/W_{C_j}(e)\}$, that is $\bar{\gamma}_e$ is computed through the actual weights $W_{C_j}(e)$ over all elements of C_j . For case (II) when $|F_{C_j}^0| = |C_j|$ the algorithm SILH-PPS-ALL relies on the values $\bar{\gamma}_e$. Let $\gamma_e, e \in C_j$ be the coefficients obtained when $F_{C_j}^0$ contains a single well-positioned element, then by Equation (6) there exists a constant c such that

$$\sum_{e \in C_j} \bar{\gamma}_e \leq c \sum_{e \in C_j} \gamma_e \leq 2c .$$

Therefore even when $|F_{C_j}^0| = |C_j|$ we have that $\sum_e \gamma_e \leq O(1)$. Note that case (III) implies that even in the highly unlikely case of $|F_{C_j}^0| = |C_j|$, the final sample F_{C_j} will be such that $\mathbb{E}[|F_{C_j}|] = O(t)$. Finally, consider case (III), when $1 < |F_{C_j}^0| < |C_j|$, and let γ_e be the coefficients obtained by SILH-PPS-ALL with $F_{C_j}^0$. By contradiction assume that $\sum_e \gamma_e > \sum_e \bar{\gamma}_e$, for $\bar{\gamma}_e$ defined as in case (II), which implies that $\sum_e \left[\max \left\{ \frac{1}{|C_j|}, \max_{\bar{e} \in F_{C_j}^0} \frac{d(e, \bar{e})}{W_{C_j}(\bar{e})} \right\} - \max \left\{ \frac{1}{|C_j|}, \max_{\bar{e} \in C_j} \frac{d(e, \bar{e})}{W_{C_j}(\bar{e})} \right\} \right] > 0$. It is simple to observe that none of the terms in the summation can be larger than 0 since $F_{C_j}^0 \subset C_j$, yielding the contradiction. Hence, we have that for each set $F_{C_j}^0, |F_{C_j}^0| \in (1, |C_j|)$ it holds that $\sum_e \gamma_e \leq \sum_e \bar{\gamma}_e \leq O(1)$, and in turn $\mathbb{E}[|F_{C_j}|] = O(t)$. Combining the above three cases we have

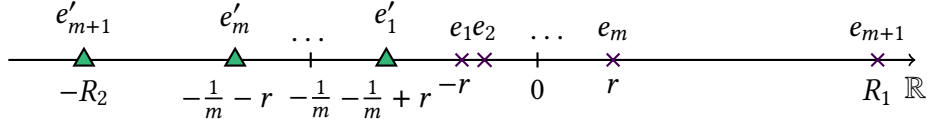


Figure 2: Instance used to prove [Theorem 2](#) (see [Section 4.1.3](#)). $C_1 = \{e_1, \dots, e_{m+1}\}$ and $C_2 = \{e'_1, \dots, e'_{m+1}\}$.

that any (random) choice of set $F_{C_j}^0$ will yield $\mathbb{E}[|F_{C_j}|] = \mathcal{O}(t)$. Applying the Chernoff bound, we obtain that $|F_{C_j}| = \mathcal{O}(t)$ with probability $1 - \delta/(5k)$ by the choice of t as from [Lemma 1](#), proving our statement. \square

Observe that the number of distance computations performed by SILH-PPS-ALL is bounded by

$$\sum_{j=1}^k |C_j| (|F_{C_j}^0| + |F_{C_j}|), \quad (7)$$

where for ease of notation $|F_{C_j}^0| = 0$ when $|C_j| \leq t$. By combining [Equation \(7\)](#), together with [Lemma 3](#), we obtain the bound on the sample size and the bound on the number of distance computations claimed in [Theorem 1](#), which hold with probability at least $1 - 2\delta/5$ —yielding [Theorem 1](#) by [Lemmas 1](#) and [2](#).

4.1.3 Proof of [Theorem 2](#)

We now show that simple Poisson sampling over each cluster C_j , $j \in [k]$, with an expected sample size equal to SILH-PPS-ALL, is *not* sufficient to obtain an accurate estimate of weights $W_{C_j}(e)$, $j \in [k]$, $e \in V$. That is, we will provide an instance of [Problem 1](#) where a *uniform* sampling technique with a sample complexity of $\Theta(tk)$, i.e., roughly the same sample size of SILH-PPS-ALL, outputs estimates of $s(e)$, $e \in V$ with constant error $\Omega(1)$ for a large fraction of elements in V , proving [Theorem 2](#). Our result shows that non-uniform sampling (e.g., PPS sampling) is necessary to get the rigorous approximation guarantees provided by our algorithm SILH-PPS-ALL.

Building the instance. Let $V = \{e_1, \dots, e_{m+1}, e'_1, \dots, e'_m, e'_{m+1}\}$, $|V| = 2m + 2$ for fixed and very large m and $C = \{C_1, C_2\}$ such that $C_1 = \{e_1, \dots, e_{m+1}\}$, $C_2 = \{e'_1, \dots, e'_{m+1}\}$ and fix d to be the Euclidean distance over $\mathbb{R} \supset V$.⁵ For ease of presentation, and without loss of generality, we assume that the elements of each cluster are ordered according to their indexing, that is $e_i < e_j$ (resp. $e'_i > e'_j$) if it holds $1 \leq i < j \leq m + 1$. The elements of C_1 are placed as follows: (i) the m elements e_i , $1 \leq i \leq m$, span an interval of length $2r$, $r = o(1/m)$, $r > 0$ centered at the origin (i.e., $d(e_i, 0) \leq r$); (ii) $e_{m+1} \geq 0$ is such that $d(e_{m+1}, 0) \geq R_1$, for some large value R_1 (that we will specify later). The structure of C_2 is similar to the structure of C_1 : the m elements e'_i , $1 \leq i \leq m$ are within an interval of length r centered at $-1/m$, and $e'_{m+1} < 0$ at distance $R_2 > 0$, $R_2 = \Theta(m)$ from 0. Furthermore, let the points e_i (resp. e'_i) for $i \in [m]$ be equally spaced over the intervals containing them, that is $d(e_i, e_{i+1})$ (resp. $d(e'_i, e'_{i+1})$) equals βr with $\beta \doteq 2/(m - 1)$, for $i \in [m - 1]$. We display the geometry of the resulting dataset in [Figure 2](#). Finally let $R_1 \geq L'(R_2 + 1)$ for arbitrary large L' .

⁵Recall for $a, b \in \mathbb{R}$ the Euclidean distance corresponds to $d(a, b) = |a - b|$, denoted also as *length*.

Proposition 1. Consider dataset V and its clustering C as constructed above. Then, for each element $e_i, i \in [m]$ there exists a large constant L such that $s(e_i) = \frac{(1-L)}{L} \approx -1$.

Proof. Fix an element from C_1 in the closed interval of radius r centered at the origin, i.e., $e_i, i \in [m]$. Then consider the value of $a(e_i), i \in [m]$ in the definition of $s(e_i)$, we have that

$$a(e_i) = \frac{W_{C_1}(e_i)}{m} = \frac{1}{m} \sum_{j=1, j \neq i}^m d(e_j, e_i) + \frac{d(e_{m+1}, e_i)}{m} \leq \frac{m-1}{m} 2r + \frac{(R_1+r)}{m} \leq \frac{R_1}{m} + 3r ,$$

by using the triangle inequality. We also have the following lower bound on $a(e_i)$,

$$a(e_i) = \frac{W_{C_1}(e_i)}{m} = \frac{1}{m} \sum_{j=1, j \neq i}^m d(e_j, e_i) + \frac{d(e_{m+1}, e_i)}{m} \geq \frac{m-1}{m} \beta r + \frac{(R_1-r)}{m} \geq \frac{R_1+r}{m} ,$$

where in the first inequality we used the fact that the distance between two elements e_i, e_j with $1 \leq i \neq j \leq m$ of C_1 is $\beta r, \beta = 2/(m-1)$ and that $d(e_{m+1}, e_i) \geq R_1 - r$. Hence $a(e_i) = R_1/m + o(1/m)$ by the fact that $r = o(1/m)$. Next for the term $b(e_i), i \in [m]$ with a similar argument we have that

$$\begin{aligned} b(e_i) &= \frac{W_{C_2}(e_i)}{m+1} = \frac{1}{m+1} \sum_{j=1}^m d(e'_j, e_i) + \frac{d(e'_{m+1}, e_i)}{m+1} \leq \\ &\leq \frac{m}{m+1} \left(\frac{1}{m} + 2r \right) + \frac{(R_2+r)}{m+1} \leq \frac{r+1}{m+1} + 2r + \frac{R_2}{m+1} . \end{aligned}$$

(e.g., by using the triangle inequality). Finally, for the lower bound,

$$\begin{aligned} b(e_i) &= \frac{W_{C_2}(e_i)}{m+1} = \frac{1}{m+1} \sum_{j=1}^m d(e'_j, e_i) + \frac{d(e'_{m+1}, e_i)}{m+1} \geq \\ &\geq \frac{m}{m+1} \left(\frac{1}{m} - 2r \right) + \frac{(R_2-r)}{m+1} \geq \frac{1-2mr-r}{m+1} + \frac{R_2}{m+1} . \end{aligned}$$

Hence $b(e_i) = (R_2+1)/(m+1) + o(1/m)$. Focusing on the dominating terms of $a(e_i)$ and $b(e_i)$ and setting $R_1 = L(R_2+1)m/(m+1)$, we have that

$$s(e_i) = \frac{(R_2+1)/(m+1) - R_1/m}{\max\{(R_2+1)/(m+1), R_1/m\}} = \frac{(1-L)(R_2+1)/(m+1)}{L(R_2+1)/(m+1)} = \frac{(1-L)}{L} = -1 + \frac{1}{L} \approx -1 .$$

□

Comparing uniform sampling with our algorithm SILH-PPS-ALL. Consider now a *uniform Poisson sampling strategy* (denoted as *uniform sampling* for short), that estimates $W_{C_j}(e), j = 1, 2$ as follows:

1. Collect a sample $S_{C_j}, j = 1, 2$ of points from each cluster, including each point with probability $p = t/|C_j| = t/(m+1), p > 0$ for $t = o(m)$ (i.e., the same t used by SILH-PPS-ALL);

2. Estimate $W_{C_j}(e)$, $j = 1, 2$ as:

$$\widehat{W}_{C_j}^U(e) = \sum_{e' \in S_{C_j}} \frac{d(e, e')}{p} = \sum_{e' \in S_{C_j}} \frac{d(e, e')(m+1)}{t} .$$

It is easy to show that the estimators $\widehat{W}_{C_j}^U(e)$ are unbiased. We can also use the estimators $\widehat{W}_{C_j}^U(e)$ to approximate the silhouette $s(e)$ in an analogous way as done in Equation (5). That is for each $e \in C_1$, we consider the estimate

$$\widehat{s}_U(e) = \frac{\widehat{W}_{C_2}^U(e)/(m+1) - \widehat{W}_{C_1}^U(e)/m}{\max \left\{ \widehat{W}_{C_2}^U(e)/(m+1), \widehat{W}_{C_1}^U(e)/m \right\}} .$$

In the next lemma, we show that for a fixed sample size $t = o(m)$ and with arbitrary large probability close to 1, it holds that $|\widehat{s}_U(e) - s(e)| \approx 2$. That is, the estimation error of the uniform sampling strategy corresponds to the *maximum error attainable*, for all $e \in C_1 \setminus \{e_{m+1}\}$. In contrast, the estimates provided by SILH-PPS-ALL, using the same value of t achieve, for $e \in C_1$, $|\widehat{s}(e) - s(e)| \approx 0$ with large probability, that can be made arbitrarily close to 1. A similar argument can be used to show a large constant estimation error for $\widehat{s}_U(e)$ over all elements in $e \in C_2$.

Proposition 2. *Let V and $C = \{C_1, C_2\}$ be the instance to Problem 1 constructed above. Then, for each element in $e_i \in C_1$ with $i \in [m]$ the value of the uniform Poisson sampling strategy yields $\widehat{s}_U(e_i) \approx 1$ while SILH-PPS-ALL yields $\widehat{s}(e_i) \approx -1$ with arbitrarily large probability. Therefore, $|s(e_i) - \widehat{s}_U(e_i)| \approx 2$, while $|s(e_i) - \widehat{s}(e_i)| \approx 0$.*

Proof. Let a be a small constant. For ease of presentation and given that m is very large, our analysis considers the following case: “the uniform Poisson sampling strategy over C_j yields at total sampled elements”. Note that since the number of samples corresponds to a Binomial distribution $\text{Bin}(m+1, t/(m+1))$ for large m , this is often the case, up to a very small constant. A similar result holds for the size of F_{C_j} , $j \in [k]$ of our algorithm SILH-PPS-ALL (see the proof of Lemma 3). Therefore, for simplicity, in our analysis we assume that both $|S_{C_j}| = |F_{C_j}| = at$, exactly. Consider the uniform sampling strategy and define the following two events $E_1 \doteq “e_{m+1}$ is not sampled in $S_{C_1}”$ and $E_2 \doteq “e'_{m+1}$ is not sampled in $S_{C_2}”$. We have that $\mathbb{P}[E_1] = \mathbb{P}[E_2] = (1 - t/(m+1)) = 1 - o(1)$ for arbitrary large m , by the choice of t . Hence, conditioning on E_1 and E_2 , we obtain that for $e \in C_1 \setminus \{e_{m+1}\}$,

$$\widehat{W}_{C_1}^U(e) \geq \frac{m+1}{t} \beta rat \geq \frac{(m+1)2ra}{(m-1)} , \quad \widehat{W}_{C_1}^U(e) \leq \frac{m+1}{t} 2rat = (m+1)2ra$$

and

$$\begin{aligned} \widehat{W}_{C_2}^U(e) &\leq \frac{m+1}{t} \left(\frac{1}{m} + 2r \right) at \leq \frac{a(m+1)}{m} + (m+1)2ra , \\ \widehat{W}_{C_2}^U(e) &\geq \frac{m+1}{t} \left(\frac{1}{m} - 2r \right) at \geq \frac{a(m+1)}{m} - a(m+1)2r . \end{aligned}$$

Hence, for m large and $r = o(1/m)$ we have that $\widehat{W}_{C_1}^U(e)$ approaches 0 while $\widehat{W}_{C_2}^U(e) = a(m+1)/m$. Therefore, focusing on the dominant terms we have that

$$\widehat{s}_U(e) = \frac{1/m}{1/m} + o(1) \approx 1 .$$

Next consider the estimates $\widehat{W}_{C_j}(e)$, $j = 1, 2$ computed by SILH-PPS-ALL. Where we condition on the events E_1 and E_2 defined over $F_{C_j}^0$. Then we have that $\gamma_e \geq \max_{\bar{e} \in F_{C_1}^0} d(\bar{e}, e) / \widehat{W}_{C_1}(\bar{e})$ for $e = e_{m+1}$ that is $\gamma_e \geq (R_1 - r) / (R_1 + r + 2mr) = 1 - o(1)$. Therefore over t points selected in the final sample F_{C_1} , point e_{m+1} will be selected with probability arbitrary close to 1 by SILH-PPS-ALL, by the choice of r . A similar argument applies to e'_{m+1} . We therefore have that for $e \in C_1 \setminus \{e_{m+1}\}$ it holds

$$\begin{aligned} \widehat{W}_{C_1}(e) &= d(e, e_{m+1}) + \sum_{e' \in F_{C_1}} \frac{d(e, e')}{p'_e} = R_1 + o(R_1) \\ \widehat{W}_{C_2}(e) &= d(e, e'_{m+1}) + \sum_{e' \in F_{C_2}} \frac{d(e, e')}{p'_e} = R_2 + o(R_2) \end{aligned}$$

by the facts that $r = o(1/m)$, $t = o(m)$, $R_2 = \Theta(m)$ and that C_2 is centered at $-1/m$. Hence, by the choice of $R_1 = L(R_2 + 1)$, for a suitably large L , focusing on the dominant terms

$$\widehat{s}(e) = \frac{R_2/(m+1) - R_1/m}{\max\{R_2/(m+1), R_1/m\}} \approx -1 .$$

The final claim follows by computing the distance of $\widehat{s}_U(e)$ and $\widehat{s}(e)$ using the exact silhouette values of e_i , $i \in [m]$ from [Proposition 1](#), i.e., $s(e) \approx -1$. \square

Proving our result. The final claim of [Theorem 2](#) follows as a corollary of [Proposition 2](#), and noting that $|V| = n = 2m + 2$ and $|C_1| = m + 1$. We remark that our result provides evidence of the superior accuracy achieved by SILH-PPS-ALL over a naive uniform Poisson sampling approach. That is, our SILH-PPS-ALL provably reports much more accurate estimates of the values of $s(e)$, $e \in V$ that cannot be matched by a uniform sampling strategy, used to approximate the values of $W_{C_j}(e)$, $j \in [k]$, when both approaches retain the same sample complexity. We further complement our theoretical insights with our extensive experimental evaluation in [Section 5](#).

4.2 Estimating the silhouette of a clustering

We now study the problem of obtaining a tight and accurate estimate of the silhouette of a clustering C , as captured in our next statement.

Problem 2. *Given a set of elements V and a k -clustering C of V and two parameters $\varepsilon, \delta \in (0, 1)$, obtain an estimator $s'(C)$ such that $|s'(C) - s(C)| \leq f(\varepsilon)$ with probability at least $1 - \delta$, minimizing the number of distance computations required to compute $s'(C)$.*

Recall that $s(C)$ is largely used in practice for evaluating the quality of a clustering C —where C is often obtained optimizing popular clustering metrics such as the k -means or k -medoids

objective functions [Dudek, 2020]. Hence, obtaining an accurate approximation of $s(C)$ is of high practical utility, e.g., for identifying a good value for the parameter k on large datasets where $s(C)$ cannot be computed exactly.

In the next sections we will obtain several estimators for the value $s(C)$, solving Problem 2, where, in analogy with Problem 1, we want $f(\varepsilon) = \Theta(\varepsilon)$. In addition, we want to output our highly accurate estimate $s'(C)$ performing significantly less distance computations required by the exact algorithm, i.e., $\Theta(n^2)$.

4.2.1 Estimator based on the silhouette definition

Our first estimator (Global-sampler, GL-S) is based on the definition of $s(C)$ itself (see Equation 3). That is, $s(C)$ corresponds to the average of the silhouette of all the elements $e \in V$, where each term $s(e)$ contributing to the average takes a value ranging from -1 to 1 . Therefore, our first estimator is based on *sampling* a sufficiently small number of elements from V , and using the average of their *exact* silhouette value (i.e., $s(e)$) as proxy for the overall silhouette $s(C)$.

The estimator is computed as follows: we sample $\{e_1, \dots, e_m\}$ *random* elements from V where each element $e_\ell, \ell \in [m]$ is sampled uniformly at random from the set V . The resulting estimator can be expressed as

$$\widehat{s}_1(C) = \frac{1}{m} \sum_{\ell=1}^m s(e_\ell) . \quad (8)$$

The next result quantifies the guarantees offered by estimator $\widehat{s}_1(C)$.

Theorem 3. *Let V be a dataset of n elements, and let C be a k -clustering of V . If $m \geq \frac{2}{\varepsilon^2} \ln \frac{2}{\delta}$, then $|\widehat{s}_1(C) - s(C)| \leq \varepsilon$ with probability at least $1 - \delta$.*

Proof. Note that $s(e_\ell), \ell = 1, \dots, m$ are random variables taking values in the interval $[-1, 1]$. Moreover, for each $\ell = 1, \dots, m$, we have that $\mathbb{E}[s(e_\ell)] = \sum_{e \in V} s(e)/n = s(C)$. The result follows directly from the application of Hoeffding's bound (Theorem 6). \square

The time complexity (i.e., number of distance computations) required to compute $\widehat{s}_1(C)$ is $O(mn)$, for fixed m .

4.2.2 Estimator using SILH-PPS-ALL

Recall that in Section 4.1 we developed our algorithm SILH-PPS-ALL that given a dataset V , a clustering C of V and two parameters $\varepsilon, \delta \in (0, 1)$ computes a set $\widehat{s}(V)$ such that for each $e \in V$ it holds $|\widehat{s}(e) - s(e)| \leq (4\varepsilon)/(1 - \varepsilon)$ with probability at least $1 - \delta$. Our second estimator (GLOBAL-PPS-Full-sampler, GL-PPS-F) approximates the silhouette $s(C)$ using the estimates $\widehat{s}(e)$ for each element $e \in V$ as obtained by SILH-PPS-ALL, that is

$$\widehat{s}_2(C) = \frac{1}{n} \sum_{e \in V} \widehat{s}(e) , \quad (9)$$

where the values $\widehat{s}(e), e \in V$ are computed by SILH-PPS-ALL. The next theorem establishes an upper bound to the absolute error of $\widehat{s}_2(C)$ with respect to $s(C)$.

Theorem 4. Let V be a dataset of n elements, and let C be a k -clustering of V . Let $\widehat{s}_2(C)$ be the estimate of the silhouette of the clustering $s(C)$ computed as in Equation (9) by running SILH-PPS-ALL for given parameters ε and δ , with $0 < \varepsilon, \delta < 1$, and for a suitable choice of the sample size t . Then, with probability at least $1 - \delta$, it holds that

$$|\widehat{s}_2(C) - s(C)| \leq \frac{4\varepsilon}{1 - \varepsilon} .$$

The proof is an immediate consequence of the definition of $s(C)$ (Equation (3)) and $\widehat{s}_2(C)$ (Equation (9)), and of the guarantees provided by Lemmas 1 and 2.

For a given (expected) sample size t ,⁶ the time complexity to compute $\widehat{s}_2(C)$ is the same required by SILH-PPS-ALL, that is $O(nkt)$ with probability at least $1 - \delta$ (see Lemma 3, and the related discussion).

4.2.3 Estimator using two-phase sampling

Let us consider, for ease of notation, the set $\widehat{s}(V) = \{\widehat{s}(e_1), \dots, \widehat{s}(e_n)\}$ of estimates computed with SILH-PPS-ALL. Note that the values in the set $\widehat{s}(V)$ are *fixed* once the PPS sampling phase of Algorithm 1 (i.e., *Phase 1*) has been performed, even if the values in $\widehat{s}(V)$ have not explicitly been computed yet.⁷ We therefore approximate the estimator in Equation (9) as follows:

1. Execute *Phase 1* of Algorithm 1 and obtain all samples $F_{C_j}, j \in [k]$, so that the values of $\widehat{s}(e_i), i \in [n]$ are determined (i.e., the set $\widehat{s}(V)$), even if not computed yet;
2. Select uniformly at random $m \in \mathbb{N}, m \geq 2$ indices i_1, \dots, i_m in the set $\{1, \dots, n\}$;
3. For each $i_j, j \in \{1, \dots, m\}$ evaluate $\widehat{s}(e_{i_j})$;
4. Return the average $\bar{s}(C)$ over the m estimates $\widehat{s}(e_{i_j})$ obtained above.

The resulting estimator (Global-PPS-sub-sampler, GL-PPS-s) can be expressed as follows,

$$\bar{s}(C) = \frac{1}{m} \sum_{j=1}^m \widehat{s}(e_{i_j}) . \quad (10)$$

The following result shows that $\bar{s}(C)$ is an unbiased estimator of $\widehat{s}_2(C)$.

Lemma 4. $\mathbb{E}[\bar{s}(C)] = \widehat{s}_2(C)$.

Proof. For each $j \in \{1, \dots, m\}$, let X_j be a random variable with value $\widehat{s}(e_{i_j})$ (observe that i_j is itself a random variable). Note that $\bar{s}(C) = \frac{1}{m} \sum_{j=1}^m X_j$. By taking expectations, using linearity, and the fact that r.v.'s i_j 's are taken uniformly at random from the set $\{1, \dots, n\}$ we have

$$\mathbb{E}[\bar{s}(C)] = \frac{1}{m} \sum_{j=1}^m \mathbb{E}[X_j] = \frac{1}{m} \sum_{j=1}^m \sum_{i=1}^n \widehat{s}(e_i) \frac{1}{n} = \frac{1}{n} \sum_{i=1}^n \widehat{s}(e_i) = \widehat{s}_2(C).$$

□

⁶Recall that the number of samples in each cluster in SILH-PPS-ALL is $O(t)$ with probability at least $1 - 2\delta/5$.

⁷After Phase 1, the values $\widehat{s}(e_1), \dots, \widehat{s}(e_n)$ are determined, i.e., there is no randomness once the samples F_{C_j} for $j \in [k]$ are fixed.

Table 1: Summary of the various estimators to approximate $s(C)$, the silhouette of a clustering C , as captured by [Problem 2](#). We label with *algorithm* the method used to evaluate each estimator. The sample size $m(\varepsilon_2, \delta_2)$ is detailed in [Lemma 5](#).

Algorithm	Estimator	Guarantees	Distance-Computations	Probability
GL-S	$\widehat{s}_1(C)$	$ \widehat{s}_1(C) - s(C) \leq \varepsilon$	$O\left(\frac{n}{\varepsilon^2} \log\left(\frac{1}{\delta}\right)\right)$	$> 1 - \delta$
GL-PPS-F	$\widehat{s}_2(C)$	$ \widehat{s}_2(C) - s(C) \leq \frac{4\varepsilon}{1-\varepsilon}$	$O\left(\frac{nk}{\varepsilon^2} \log\left(\frac{nk}{\delta}\right)\right)$	$> 1 - \delta$
GL-PPS-S	$\bar{s}(C)$	$ \bar{s}(C) - s(C) \leq \frac{4\varepsilon_1}{1-\varepsilon_1} + \varepsilon_2$	$O\left(\left(n + \frac{m(\varepsilon_2, \delta_2)k}{\varepsilon_1^2}\right) \left(\log\left(\frac{nk}{\delta_1}\right)\right)\right)$	$> (1 - \delta_1)(1 - \delta_2)$

The following result provides the guarantees on the approximation of $\widehat{s}_2(C)$ provided by its estimator $\bar{s}(C)$.

Lemma 5. Fix $(\varepsilon_2, \delta_2) \in (0, 1)^2$ then if $m \geq \frac{2}{\varepsilon_2^2} \ln\left(\frac{2}{\delta_2}\right)$ then $\mathbb{P}[|\widehat{s}_2(C) - \bar{s}(C)| \geq \varepsilon_2] \leq \delta_2$.

Proof. First recall variables $X_j, j \in [1, m]$ are bounded in the range $[-1, 1]$. Then combining the proof of [Lemma 4](#) showing that for each $j \in [m]$, $\mathbb{E}[X_j] = \widehat{s}(C)$ and Hoeffding's bound ([Theorem 6](#)) we have that

$$\mathbb{P}[|\bar{s}(C) - \widehat{s}_2(C)| \geq \varepsilon_2] \leq 2 \exp\left(-\frac{2m\varepsilon_2^2}{4}\right) \leq \delta_2,$$

where the last step is by the choice of m as in statement. \square

We now prove the resulting error obtained from approximating the silhouette $s(C)$ with $\bar{s}(C)$.

Lemma 6. Fix $(\delta_1, \delta_2) \in (0, 1)^2$ then $|s(C) - \bar{s}(C)| \leq \varepsilon_1 + \varepsilon_2$ with probability at least $(1 - \delta_1)(1 - \delta_2)$, where ε_1 is the bound on the error obtained in [Theorem 4](#) on $\widehat{s}_2(C)$ and $s(C)$ w.p. $1 - \delta_1$, and ε_2 is a bound on the error between $\bar{s}(C)$ and $\widehat{s}_2(C)$ obtained with Hoeffding's inequality as in [Lemma 4](#) w.p. at least $1 - \delta_2$.

Proof. Note that $|s(C) - \widehat{s}_2(C)| \leq \varepsilon_1$ and $|\widehat{s}_2(C) - \bar{s}(C)| \leq \varepsilon_2$ hold respectively w.p. $(1 - \delta_1)$ and $(1 - \delta_2)$, and that such events are independent. Therefore by the triangle inequality,

$$|s(C) - \bar{s}(C)| = |s(C) \pm \widehat{s}_2(C) - \bar{s}(C)| \leq |s(C) - \widehat{s}_2(C)| + |\widehat{s}_2(C) - \bar{s}(C)| \leq \varepsilon_1 + \varepsilon_2,$$

and such event holds with probability at least $(1 - \delta_1)(1 - \delta_2)$. \square

It now remains to control $|s(C) - \bar{s}(C)| \leq \varepsilon_1 + \varepsilon_2$ to hold with probability at least $1 - \delta$ within user defined accuracy and confidence $\varepsilon, \delta \in (0, 1)$. Since the final error is bounded by $\varepsilon_1 + \varepsilon_2$ we can set $\varepsilon_2 = \varepsilon - \varepsilon_1$. Noting that $\varepsilon_1 \leq 4\varepsilon'/(1 - \varepsilon')$ it is sufficient to set $\varepsilon' = \varepsilon/q, q > 4$. Finally to control the confidence we can set $\delta_1 = \delta/2$ and $\delta_2 = \delta/(2 - \delta)$, yielding to the desired confidence to be at least $1 - \delta$ —solving [Problem 2](#) as desired.

When performing Phase 1 of SILH-PPS-ALL for a fixed t , the time complexity to compute $\bar{s}(C)$ is at most $O(n \log(nk/\delta) + mkt)$. That is the sum of the time complexity of Phase 1 (i.e., $O(n \log(nk/\delta))$) and the time complexity of running Phase 2 of SILH-PPS-ALL only for the m elements $e_{i_j}, j \in \{1, \dots, m\}$ (i.e., $O(mkt)$).

We provide a summary of our sampling techniques designed to solve [Problem 2](#) in [Table 1](#).

4.3 Distributed algorithms

In this section, we present a distributed design of our silhouette approximation algorithms (i.e., both for local and global estimation) using the MapReduce framework [Dean and Ghemawat, 2008, Leskovec et al., 2014, Pietracaprina et al., 2012]. At the end of the section, we will briefly discuss how to simply adapt our design to the popular MPC model [Beame et al., 2017, Im et al., 2023, Karloff et al., 2010].

4.3.1 Computational model

MapReduce adopts a functional programming model where an algorithm is specified as a sequence of *rounds*. In each round:

1. a multiset X of key-value pairs is first transformed into a new multiset X' of key-value pairs by applying a *map function* independently to each pair (possibly in parallel);
2. the multiset X' is then transformed into a multiset Y of pairs by applying a *reduce function* independently to each subset of key-value pairs of X' sharing the same key (possibly in parallel);
3. the multiset of key-value pairs Y is then used as an input to the subsequent round, if any.

Throughout the description of our algorithms, a key-value pair will be denoted as $(key \mid value_1, \dots, value_r)$, where $\langle value_1, \dots, value_r \rangle$ corresponds to an r -dimensional *value*, for (a small) constant r . As customary in the MapReduce literature Leskovec et al. [2014], we use the term *reducer* to refer to the application of a reduce function to a set of pairs with the same key, i.e., see step (2) in the above discussion.

When a MapReduce algorithm is executed in a distributed environment, the instances of the map (resp., reduce) functions of a round are assigned by the underlying system to the available computing nodes. That is, a MapReduce algorithm is agnostic to the actual number of computing nodes. Therefore, important performance indicators to be minimized for a MapReduce algorithm are: *i*) the number of rounds; *ii*) the maximum amount M_L of *local memory* required by any instance of the map or reduce functions; *iii*) the maximum amount M_A of *aggregate memory* required at *any* round to store the input, output and intermediate data.

In our setting, consider a k -clustering $\mathcal{C} = \{C_1, \dots, C_k\}$ of a dataset $V = \{e_0, \dots, e_{n-1}\}$ of n elements, and assume that each element $e \in V$ has additional information $C(e)$ denoting the cluster to which $e \in V$ is assigned to over \mathcal{C} . Initially, we represent the input clustering by the following set of key-value pairs:

$$\{(i|e_i) : 0 \leq i < n\} .$$

Reasonably, we assume that the values n , k , and t used in the MapReduce algorithm, and the size $|C_j|$ for each $j \in [k]$, are known globally. A key ingredient of our design is that in each round, the elements of V , and the newly created intermediate data, will be partitioned into w subsets of size n/w each, where $w \in [0, n - 1]$ is a suitable design parameter. To simplify the description and the analysis of our methods, we assume that $w \in \mathcal{O}(n^\alpha)$, for some (small) $\alpha < 1/2$. While our methods can be generalized to larger values of w (i.e., those corresponding to $\alpha \geq 1/2$) with minimal modifications, we highlight that w constitutes an upper bound to the maximum *parallelism* exploitable by the algorithm. Thus, assuming that $w \in \mathcal{O}(\sqrt{n})$ does not constitute a limitation in practice, especially for modern datasets of massive size n .

4.3.2 Approximating the silhouette of each element

We now present how to adapt our algorithm SILH-PPS-ALL to the MapReduce framework. Our method requires 3 rounds: the first two rounds obtain the sample F_{C_j} , for every cluster C_j and $j \in [k]$, while the last round computes the estimates $\widehat{s}(e)$ of $s(e)$ of each element $e \in V$.

Round 1.

- **Map.** Map each pair $(i|e_i)$ into the pair $(i \bmod w|e_i, 0)$. In addition, if $|C(e_i)| > t$ then, with probability $(2/|C(e_i)|) \ln(2k/\delta)$, select e_i to be part of the initial Poisson sample $F_{C(e_i)}^{(0)}$, producing w additional pairs $(\ell|e_i, 1)$, with $0 \leq \ell < w$.
- **Reduce.** For $0 \leq \ell < w$, the reducer associated with key ℓ has a copy of all initial samples $F_{C_j}^{(0)}$ (represented by the pairs $(\ell|e_i, 1)$) and a subset V_ℓ of V (represented by the pairs $(\ell|e_i, 0)$). Observe that the sets $V_\ell, \ell \in [0, w)$ form a balanced partition of V into w subsets. Then, for each element $e_i \in F_{C(e_i)}^{(0)}$, the reducer computes the term $W_{i,\ell}$, defined as the sum of distances from e_i to all elements of $V_\ell \cap C(e_i)$ producing the pair $(\ell|e_i, W_{i,\ell}, 1)$. In addition, for each pair $(\ell|e_i, 0)$ produce the pair $(\ell|e_i, 0, 0)$.

Round 2.

- **Map.** Map each pair $(\ell|e_i, W_{i,\ell}, 1)$ into the w pairs $(0|e_i, W_{i,\ell}, 1), (1|e_i, W_{i,\ell}), \dots, (w-1|e_i, W_{i,\ell}, 1)$, and each pair $(\ell|e_i, 0, 0)$ into itself.
- **Reduce.** For $0 \leq \ell < w$, the reducer associated with key ℓ has the following pairs: for every element e_i belonging to the initial sample $F_{C(e_i)}^{(0)}$ of its cluster, w pairs $(\ell|e_i, W_{i,\ell'}, 1)$, with $0 \leq \ell' < w$; and for every $e_i \in V_\ell$, a pair $(\ell|e_i, 0, 0)$. The reducer first computes $W_{C(e_i)}(e_i)$, for each element $e_i \in F_{C(e_i)}^{(0)}$, by summing all $W_{i,\ell'}$'s. Next, for each $e_i \in V_\ell$ it produces the pair $(\ell|e_i, p(e_i))$, where: 1) if $|C(e_i)| \leq t$, then $p(e_i) = 1$; otherwise 2) $p(e_i)$ is computed in terms of the $W_{C(e_i)}(e)$ with $e \in F_{C(e_i)}^0$, as specified in [Line 1](#) of [Algorithm 1](#).

Round 3.

- **Map.** Map each pair $(\ell|e_i, p(e_i))$ into the pair $(\ell|e_i, p(e_i), 0)$. In addition, with probability $p(e_i)$ select e_i to be part of the Poisson sample F_{C_j} producing pairs $(\ell'|e_i, p(e_i), 1)$, with $0 \leq \ell' < w$.
- **Reduce.** For $0 \leq \ell < w$, the reducer associated with key ℓ has a copy of all samples F_{C_j} (represented by the pairs $(\ell|e_i, p(e_i), 1)$) and the subset V_ℓ (represented by the pairs $(\ell|e_i, p(e_i), 0)$). Then, for each $e_i \in V_\ell$, the reducer computes the estimate $\widehat{s}(e_i)$, and generates the pair $(0|e_i, \widehat{s}(e_i))$ to be reported in output.

Recall that [Lemma 3](#) states that with probability at least $1 - 2\delta/5$, for every cluster C_j with $|C_j| > t$, $|F_{C_j}^0| = \mathcal{O}(\ln(k/\delta))$ and $|F_{C_j}| = \mathcal{O}(\varepsilon^{-2} \ln(nk/\delta))$. Then, since $t = \mathcal{O}(\varepsilon^{-2} \ln(nk/\delta))$, it immediately follows that, with probability at least $1 - 2\delta/5$ the maximum local memory required by any map or reduce phase in any of the above rounds is bounded by $M_L = \mathcal{O}(n/w + w + k\varepsilon^{-2} \ln(nk/\delta)) = \mathcal{O}(n/w + k\varepsilon^{-2} \ln(nk/\delta))$ and the aggregate memory is bounded by $M_A = \mathcal{O}(wM_L)$.

4.3.3 Approximating the silhouette of a clustering

In [Section 4.2](#), we introduced three methods for computing an approximation $\widehat{s}(C)$ to the silhouette of the entire clustering C , see [Table 1](#). The two estimators $\widehat{s}_2(C)$ (see [Equation \(9\)](#)) and $\bar{s}(C)$ (see [Equation \(10\)](#)), can be computed through simple aggregations of all, or an m -sample,

of the individual silhouettes estimates $\widehat{s}(e)$ for $e \in V$. These two estimators can be computed in MapReduce through a straightforward adaptation of the 3-round algorithm described above, combining, in the reduce phase of the third round, the individual silhouette estimates (or the sample ones) within each of the w partitions, and then combining the resulting values in an extra round. Overall, this 4-round approach would use the same local and aggregate space bounds obtained in Section 4.3.2. Finally, concerning the sampling method that computes $\widehat{s}_1(C)$ based on Equation (8), it can be simply implemented through the MapReduce framework, we omit the details for brevity, since the resulting approach is analogous to the techniques already introduced. Such final approach uses $\mathcal{O}(1 + (\log w / \log(n/w))) = \mathcal{O}(1)$ rounds, local memory $M_L = \mathcal{O}(n/w + k\varepsilon^{-2} \ln(1/\delta))$ and aggregate memory $M_A = \mathcal{O}(wM_L)$,

4.3.4 Porting MapReduce algorithms to the MPC framework

The MPC framework models a parallel system with p machines, each equipped with a local memory of size s . Similar to MapReduce, the computation is structured as a sequence of synchronous rounds. In a round, each machine (1) performs an arbitrary amount of computation on its local data in memory; (2) exchanges point-to-point messages with other machines. The MPC framework allows *arbitrary* communication patterns, subject to the only constraint that each machine may send or receive *at most* s point-to-point messages in each round, with messages sent in a round processed by their recipients in the next round. Similarly to MapReduce, the ultimate goal is to design MPC algorithms that run in as few rounds as possible, using local memory (heavily) sublinear in the aggregate memory size. However, MPC and MapReduce differ in the way they express parallelism: *i*) a MapReduce computation is purely functional and exhibits, at each round, a degree of (virtual) parallelism equal to the number of instances of the map and reduce functions active in the round; in contrast *ii*) an MPC computation has fixed parallelism p throughout all rounds.

It is simple to observe that the MapReduce algorithms described above (for both local and global silhouette estimation) do not rely on the dynamic parallelism offered by the MapReduce model. That is, in every round, the algorithms always partition the data into w disjoint subsets, and the computation essentially involves: *i*) local operations within each partition; *ii*) broadcast of individual elements to all partitions; *iii*) summing w contributions, one per partition. As a consequence, our algorithms can be immediately adapted to the MPC framework by associating one machine per partition, setting $p = w$ and $s = M_L$. Finally, since in our setting $M_L = \Omega(n^{1/2})$, all the required broadcast and aggregation operations can be performed in constant rounds using standard MPC techniques [Czumaj et al., 2025]. Thus, the overall number of rounds remains constant.

The following theorem, whose proof is a direct consequence of all the arguments developed in this section, provides a quantitative characterization of the performance of our distributed strategies.

Theorem 5. *There exist MapReduce and MPC algorithms providing distributed implementations of SILH-PPS-ALL, for local silhouette estimation, and of all our algorithms for global silhouette estimation from Table 1. For fixed $\varepsilon, \delta \in (0, 1)$, $w = \Theta(n^\alpha)$, for $\alpha \leq 1/2$, and $k = \mathcal{O}(n^{1-\alpha} / \log^2(n))$, our distributed algorithms require a constant number of rounds, sublinear local memory $M_L = \Theta(n^{1-\alpha})$, and linear aggregate memory, with probability at least $1 - 2\delta/5$.*

5 Experimental evaluation

In this section, we present the results of our extensive experimental evaluation. We start by describing the setup of our experiments (Section 5.1), and then we investigate the following issues.

- **I1.** Compare our new estimators (from Section 4.2) for the global silhouette $s(C)$ with state-of-the-art baselines, studying the trade-offs between accuracy and efficiency exhibited by our estimators (Section 5.2).
- **I2.** Evaluate the accuracy of our algorithm SILH-PPS-ALL for the estimation of all local silhouette values $s(e)$, for each element $e \in V$ (Section 5.3).
- **I3.** Study the scalability of a distributed implementation of our algorithm SILH-PPS-ALL (Section 5.4).
- **I4.** Illustrate applications of our new algorithms: 1. our SILH-PPS-ALL algorithm provides highly accurate *local* estimates that can be used to visualize accurate silhouette plots; 2. our *global* estimates can be used for the accurate selection of a good value of the parameter k of a k -clustering method (Section 5.5).

5.1 Setup

5.1.1 Methods and baselines

We now introduce all methods considered in our experiments. We distinguish between methods for *global* (Problem 2) and *local* estimation (Problem 1) of silhouette values.

Global estimates. We compared our algorithms with two state-of-the-art baseline algorithms. In addition, we also considered a variant of our methods coupled with uniform sampling (see Section 4.1.3). The list of methods is as follows.

- Algorithms GL-S, GL-PPS-F, and GL-PPS-S (from Table 1), which compute the estimators in Equations (8) to (10), respectively, using PPS sampling to estimate individual silhouette values.
- Two algorithms, dubbed GL-UNI-F and GL-UNI-S, which compute the estimators in Equations (9) and (10), respectively, using uniform sampling (rather than PPS sampling) to estimate all individual silhouettes (see Section 4.1.3).
- “FS” by Frahling and Sohler [2008], which, for each element $e \in V$ computes the term $a(e)$ according to its definition (Equation (2)), while estimates the term $b(e)$ as $1/|C_{\mu_e}| \sum_{e' \in C_{\mu_e}} d(e', e)$, where C_{μ_e} corresponds to the cluster with closest center (or centroid) to $e \in V$, different from the cluster C of e . Observe that the estimate of $b(e)$ is simplified with respect to the one proposed in the original paper. That is, we do not verify if the computed estimate is smaller than all the distances between e and all centers (or centroids) of the clusters in $C \setminus \{C_{\mu_e}\}$ —to avoid performing an exact computation of $b(e)$ when the check fails.
- “SIMPL” by Hruschka et al., the simplified silhouette approach, which evaluates the silhouette $s(e)$ of each element $e \in V$ using the distances of e to the closest centers (or

Table 2: Datasets used in our experiments. For each dataset, the first three columns report its name and label, its size n , and the dimensionality z of its elements (i.e., $e \in \mathbb{R}^z$). Column “exact” indicates whether the $\Theta(n^2)$ exact algorithm could be run within the allotted time limit; Column “ k -med” indicates whether the dataset could be clustered with k -medoids, under the distances listed in Section 5.1.2; and Column “size” labels the dataset as small (S), medium (M) or large (L), used in our discussion.

Name (label)	n	z	exact	k -med	size	Name (label)	n	z	exact	k -med	size
Breast (BR)	568	30	✓	✓	S	BioKDD (BioKDD)	146 K	74	✓	✗	L
Wine (WI)	6.5 K	11	✓	✓	S	RNA-seq (RNA)	489 K	8	✗	✗	L
Credit (CR)	30 K	23	✓	✓	M	Metro (MT)	1.5 M	7	✗	✗	L
Shuttle (SHU)	58 K	9	✓	✓	M	PowerHouse (PH)	2.1 M	7	✗	✗	L
IoT (IOT)	123 K	78	✓	✓	M	Gowalla (GOW)	6.4 M	2	✗	✗	L

centroids) as proxies of the average distances. Formally, let μ_1, \dots, μ_k the centers of clusters $C_1, \dots, C_k \in \mathcal{C}$ then for an element e in some cluster C the method SIMPL evaluates $a(e) = d(e, \mu)$ where μ is the center of C , and $b(e) = \min_{C_j \neq C} d(e, \mu_j)$.

Note that both the methods FS and SIMPL are deterministic, and do not offer quantitative guarantees on their estimation error, in contrast with our approaches from Table 1, where the estimation error can be controlled as a function of the input parameters.

Local estimates. When solving Problem 1 we will compare our method SILH-PPS-ALL with the uniform-sampling based approach detailed in Section 4.1.3, that we denote by UNI. That is, we do not consider FS that scales poorly on large data (our main focus for Problem 1), and SIMPL, which has very high estimation errors.

5.1.2 Datasets

A summary of the datasets used in our experiments, and their statistics is reported in Table 2. We provide more details of the processing of each dataset in Section C.1. We use small-size datasets (those marked with S in Table 2) and CR to showcase applications of Problems 1 and 2 (see Section 5.5). As for medium-size datasets, they are mainly used in Section 5.2 and Section 5.3, and are processed as follows. We cluster each dataset using both the k -means and the k -medoids objectives. For the k -means objective we consider the Euclidean distance $d_{\text{euc1}}(x, y) = \sqrt{\sum_i (x_i - y_i)^2}$. For the k -medoids objective, in addition to d_{euc1} , we also consider several widely used distance functions:

- d_{cos} , the cosine distance $d_{\text{cos}}(x, y) = 1 - \sum_i (x_i - y_i) / (\sqrt{\sum_i x_i^2} \sqrt{\sum_i y_i^2})$;
- d_{manh} , the Manhattan distance $d_{\text{manh}}(x, y) = \sum_i |x_i - y_i|$;
- d_{can} , the Canberra distance $d_{\text{can}}(x, y) = \sum_i |x_i - y_i| / (|x_i| + |y_i|)$.

For each clustering objective (either k -means or k -medoids) and each distance, we use different values of the parameter $k \in \{2, 5, 10, 15, 20\}$ to obtain different clusterings \mathcal{C} . Hence,

each distinct configuration (dataset, value of k , distance, objective) leads to a different clustering C , which we use as an input to either [Problem 2](#) or [Problem 1](#).

Finally, for the large datasets from [Table 2](#) we proceeded similarly to the medium-sized datasets, but we only clustered such data using the k -means objective to obtain different clusterings C varying k , with $k \in \{2, 5, 10, 15, 20\}$. We do not use k -medoids given its well-known poor scalability on large data.

5.1.3 Environment and parameters

We provide extensive details on the setup of the experiments in [Section C.2](#). The code to reproduce our results is available online.⁸

For our experiments, we set a time limit of one-hour for the execution of each method on a given configuration. Unless otherwise specified, each algorithm was executed for 10 independent runs and the results show the average over the runs. For our approximate algorithms, we directly set the parameter t controlling the expected sample size, rather than obtaining t as a function of the other parameters (see [Algorithm 1](#)). When comparing the algorithms from [Table 1](#) for [Problem 2](#), and their UNI variant, we will set their parameters to have a comparable runtime: we fix t for GL-PPS-F and GL-UNI-F and we set the sample size m of GL-S to kt . Unless otherwise stated we set $\delta = 0.01$.

5.1.4 Exact silhouette scores

For the small and medium sized datasets from [Table 2](#) we were able to compute the exact silhouette scores on all the various configurations described in [Section 5.1.2](#) within one hour of computation. In contrast on large data, we were not able to obtain the exact silhouette scores of any of the multiple configurations within one-hour time limit. To obtain a good proxy for the exact values of $s(e)$ for each element $e \in V$, we then proceed as follows. We perform five independent executions of SILH-PPS-ALL and its uniform variant (UNI) from [Section 4.1.3](#), obtaining respectively $\widehat{s}(e)_i$ and $\widehat{s}_U(e)_i$ with $i \in \{1, \dots, 5\}$ with a high sample size of $t = 800$. We then estimate $s(e) = (1/10) \sum_i (\widehat{s}(e)_i + \widehat{s}_U(e)_i)$ to reduce the bias in the final result.

5.2 Global silhouette approximation

In this section we evaluate the accuracy of the various methods and baselines described in [Section 5.1.1](#). We compare all methods considering the average error $|\widehat{s}(C) - s(C)| \in [0, 2]$ over ten independent runs (see [Section 5.1.3](#) for details), where $\widehat{s}(C)$ corresponds to the approximation provided by the method. In our discussion we also mention the *relative* approximation error that corresponds to $|\widehat{s}(C) - s(C)|/s(C)$. For medium-sized datasets we set the parameters of the various methods (see [Table 3](#)) as: $t = 16$ for both GL-PPS-F and GL-UNI-F, $m = \lceil n/20 \rceil$, $t = 16$ for GL-PPS-S and GL-UNI-S, and the sample size of GL-S to $m' = tk$ depending on C (see [Section 5.1.3](#)). Our choice of a small value of t is motivated by the size of our datasets, while the choice of m enforces the computation of the estimator in [Equation \(10\)](#) on a strictly sublinear number of elements in n .

⁸<https://github.com/iliesarpe/ScalableSilhouetteComputation>.

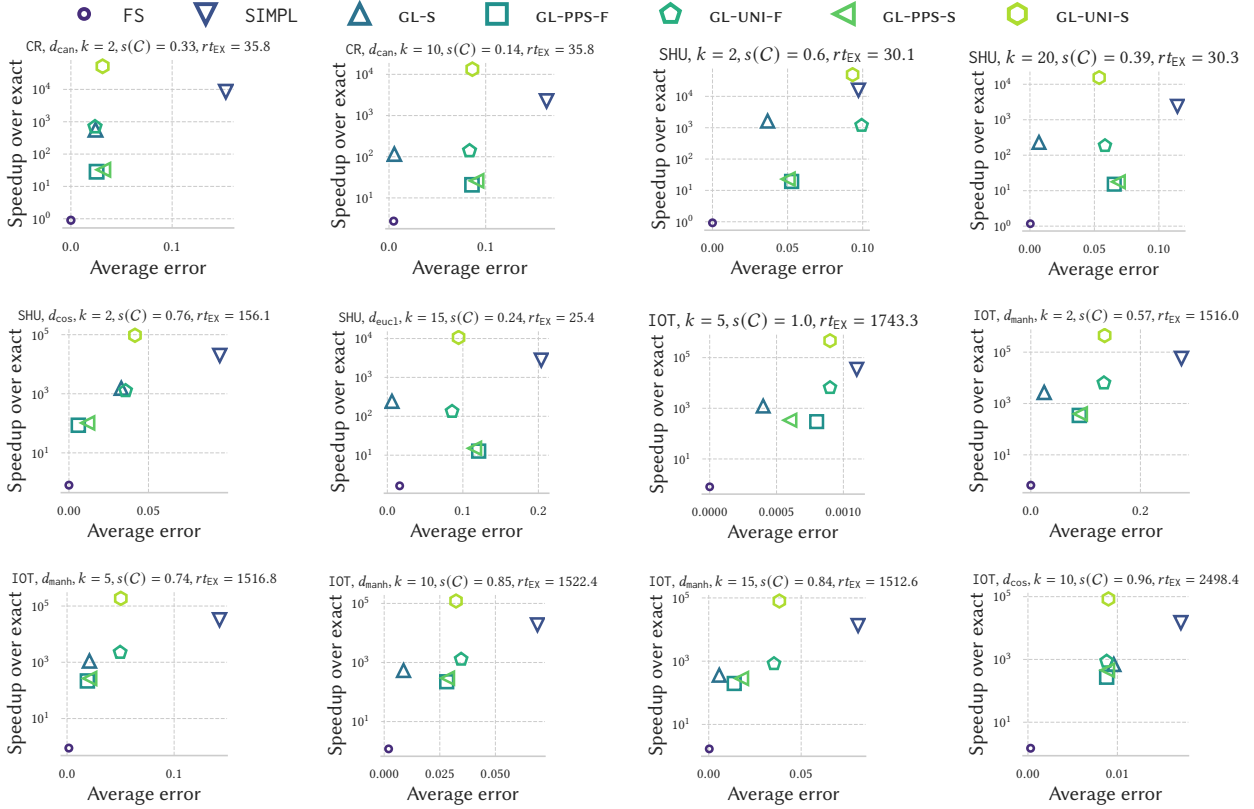


Figure 3: Trade-off between accuracy and efficiency over medium sized datasets (see Table 2). The x axis is associated with the average error over 10 independent runs, while the y axis is associated with the average speed-up over the exact computation. For each plot that corresponding to a different configuration, we report: the dataset, the distance function (when k -medoids was used to obtain the input clustering C), the value k , the exact silhouette $s(C)$, and the runtime of the exact algorithm rt_{EX} .

5.2.1 Medium datasets

We show some representative results in Figure 3, where we report the trade-off between the estimation error, and the speed-up achieved over the exact computation of the silhouette coefficient by the various methods over ten runs.

We start by observing that the FS method has a very high runtime almost matching the exact algorithm. The only configuration where the speedup is more than $3\times$, with respect to the exact approach, is the one relative to the CR dataset with d_{can} and $k = 10$. Such behavior is not surprising since, for small k , it is likely that some clusters have roughly linear size, hence FS will need a quadratic number of distance computations to compute the exact $a(e)$'s. This makes the FS method not practical on large or medium sized data, since it scales poorly. Interestingly, we note that even if the FS method is a heuristic approach (not offering guarantees), it often produces estimates with the smallest error among all methods evaluated. This is due to the fact that, for our datasets and configurations, the cluster minimizing the term $b(e)$, $e \in V$ often corresponds to the cluster with the closest center in C to e .

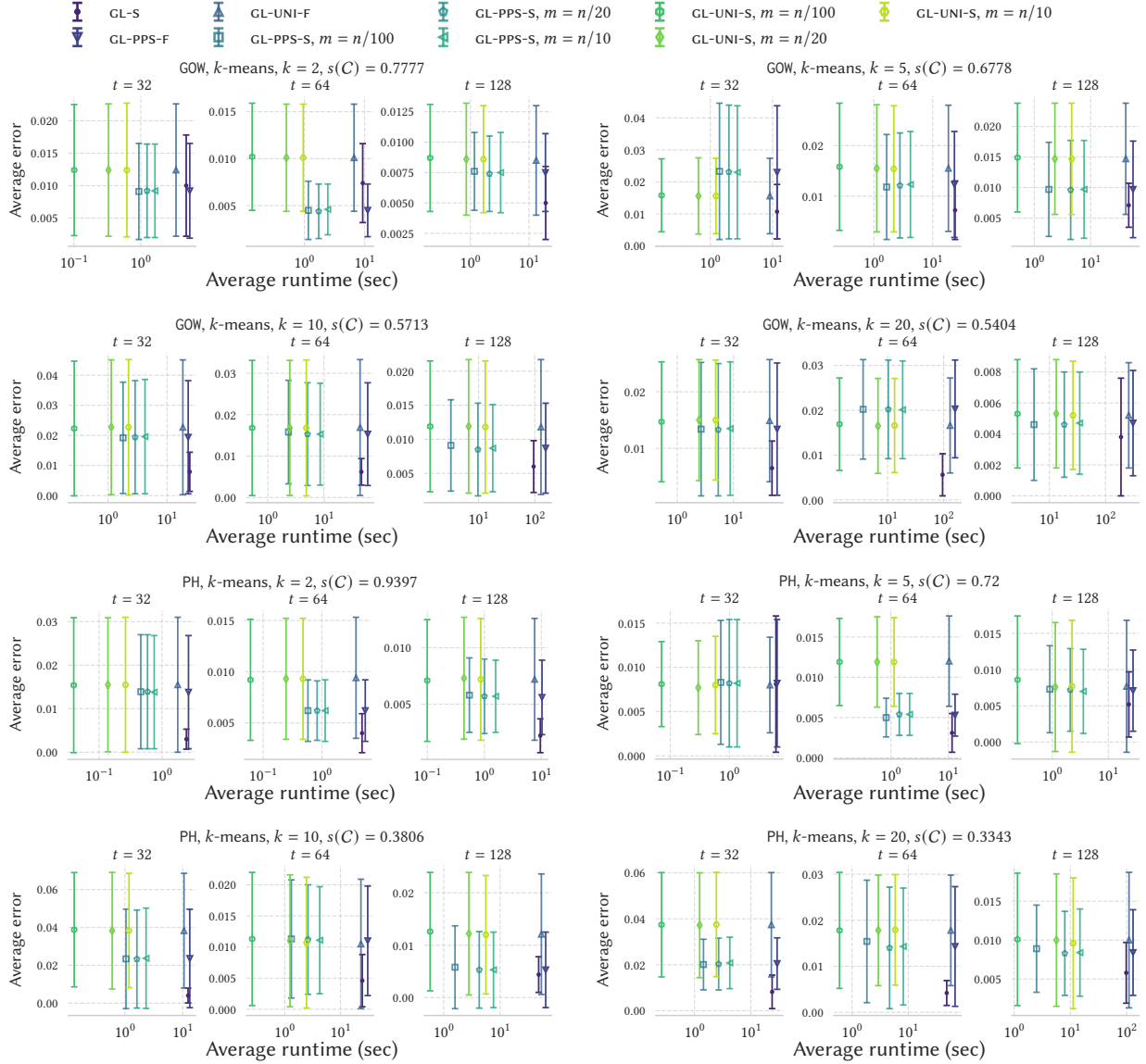


Figure 4: Methods comparison. The x axis (in log scale) is associated with the average runtime, and the y axis with the average error (and its standard deviation) over 10 independent runs. For each clustered dataset we considered different values of the expected sample size $t \in \{32, 64, 128\}$.

Next, we note that the SIMPL method is often the fastest approach among all methods we compared (except on the SHU data clustered with k -means and $k = 2$). Unfortunately, SIMPL is also the method with the largest approximation errors, which cannot be controlled by any parameter. For example, on the SHU data clustered with k -medoids and distance d_{eucl} the exact silhouette is $s(C) = 0.24$, while SIMPL outputs an estimate with an absolute error of 0.2, implying a relative error of more than 80%. Similarly, for the CR data clustered with k -medoids, d_{can} and $k = 10$, where the relative approximation error of SIMPL is more than 105%. Such large errors hinder the use of the SIMPL method in practice.

Concerning the randomized sampling algorithms we observe that GL-S often achieves the smallest estimation error compared to GL-PPS-F and GL-UNI-F—under our setting of parameters all three algorithms perform the same number of distance computations in expectation. Interestingly, for some inputs such as CR (with d_{can} and $k = 2$), SHU (with d_{cos} and $k = 2$), or IOT (with d_{cos} , $k = 10$), our new GL-PPS-F and GL-PPS-S methods achieve small approximation errors, better than GL-S, while being slightly less efficient. Comparing GL-PPS-F and GL-UNI-F, the former often achieves smaller approximation errors with respect to the latter (e.g., on the SHU data with k -means and $k = 2$, or on the IOT data on most configurations). Such a higher accuracy, comes at the expense of a higher runtime. Interestingly, we observe significant differences in runtime only on medium-sized data. This is probably caused by the fact that Phase 1 of GL-PPS-F has a non-negligible runtime compared to Phase 2 on medium-sized data such as IOT. Finally, we observe that both methods GL-PPS-S and GL-UNI-S retain the approximation guarantees offered by GL-PPS-F and GL-UNI-F, respectively, while often improving slightly (for GL-PPS-S) or significantly (for GL-UNI-S) the runtime required to evaluate the estimates.

5.2.2 Large datasets

For the experiments on large datasets, we clustered each dataset with k -means and distance d_{eucl} . We did not consider baseline FS for its poor scalability and the SIMPL method for its poor quality estimates (see Section 5.2.1). In addition, we used highly accurate estimates of $s(C)$ as ground truth, given the poor scalability of the exact computation (see Section 5.1.4).

The results are reported in Figure 4. First, as expected, all algorithms exhibit increasing accuracy as the sample size t grows. For example, on dataset GOW with $k = 5$, the error with $t = 128$ for GL-PPS-F is less than half the error obtained with $t = 32$. Next, regarding the trade-off between runtime and accuracy of GL-S, GL-PPS-F and GL-UNI-F, which perform the same expected number of distance computations, we observe several interesting trends. In almost all cases GL-S exhibited the highest accuracy and smallest variance, while GL-PPS-F provided more accurate estimates with (often significantly) smaller variance compared to GL-UNI-F.

For what concerns GL-PPS-S and GL-UNI-S, which compute the estimators of GL-PPS-F and GL-UNI-F respectively, using only a sample of size m of the total elements n , we observe that a small sample ($m = n/20$) is often sufficient to retain the accuracy of GL-PPS-F and GL-UNI-F. In addition, both GL-PPS-S and GL-UNI-S achieve remarkable speedups of up to 10× over GL-PPS-F, GL-UNI-F and GL-S. As in the case of medium datasets, the runtime of GL-PPS-S is slightly higher than the one of GL-UNI-S given the overhead introduced by Phase 1 of Algorithm 1.

Summary for issue I1. Our experiments show that neither FS nor SIMPL are suitable for estimating the global silhouette of a clustering, especially for large datasets. While FS features

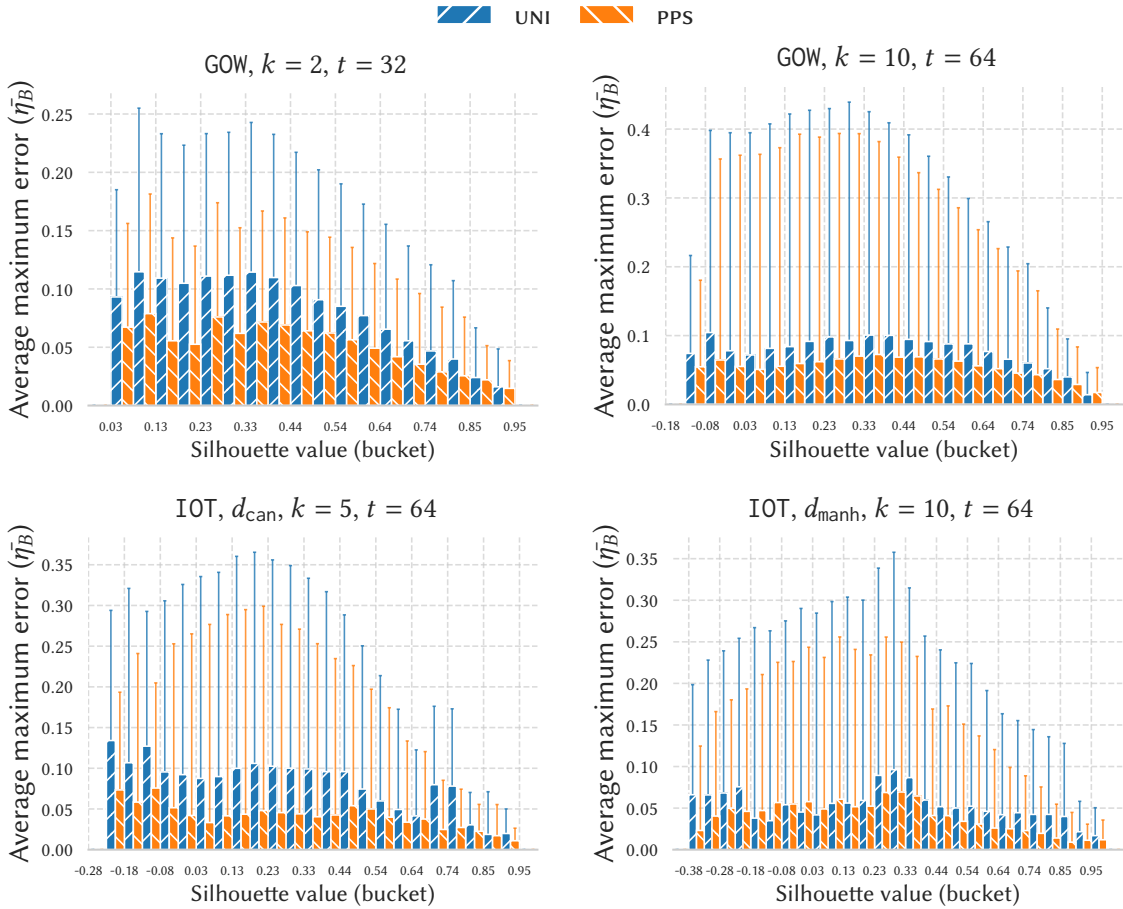


Figure 5: Plots of the average maximum error and its standard deviation obtained on all elements $e \in V$, grouped by bucket, for PPS and UNI, over four configurations. When we report the distance, it indicates that the dataset has been clustered with k -medoids. For ease of visualization we only display the average maximum error over non-empty buckets.

good accuracy, it does not yield significant speedups over the exact algorithm. On the other hand, SIMPL is very fast but it incurs high approximation errors, which cannot be controlled by any parameter.

As for randomized methods, GL-S often achieves the best trade-off between accuracy and runtime compared with GL-PPS-F and GL-UNI-F. GL-PPS-F features better accuracy compared to GL-UNI-F, at the expense of a higher runtime on most datasets. GL-PPS-S (resp., GL-UNI-S) attains comparable accuracy to GL-PPS-F (resp., GL-UNI-F) even when processing a small number of elements m compared to n —yielding a significant speedup on large datasets.

Therefore, for large datasets, where the exact computation of $s(C)$ is impractical even for a single and fixed value of k , our methods as well as GL-S provide accurate estimates efficiently. For example, on the GOW data, which has more than 6 million elements, GL-PPS-F or GL-PPS-S with $m = n/10$ and $t = 128$ output very accurate silhouette estimates for *all* values of $k \in \{2, 5, 10, 20\}$ in less than five minutes and one minute, respectively.

5.3 Local silhouette estimation

We now validate our algorithm SILH-PPS-ALL that estimates all values of $s(e), e \in V$, so to deal with issue **I2**. For ease of notation we denote SILH-PPS-ALL with PPS. As baseline we consider the uniform Poisson-sampling method, that we denote with UNI, which computes $\widehat{s}_U(e), e \in V$ using uniform Poisson sampling over each cluster $C \in \mathcal{C}$ (see [Section 4.1.3](#)). For each dataset and value of k considered in [Section 4.2](#), we evaluate the accuracy of the local estimates in two settings. First, we consider a bucketing of the values of silhouette $s(e), e \in V$. That is, we assign each element $e \in V$ to a bucket based on its silhouette value $s(e)$ where each bucket B_i , with $i = 1, \dots, 40$, corresponds to elements e with $s(e) \in [L_i, U_i)$, where $L_i = -1 + (i - 1)/20$ and $U_i = -1 + i/20$.⁹ We use the buckets B_i to evaluate the accuracy of the local estimates over each individual bucket. Second, we also analyze the accuracy of the PPS and UNI approaches over each individual cluster C_1, \dots, C_k in \mathcal{C} .

5.3.1 Accuracy over buckets

For each bucket B_i let $E_i \subseteq V$ be the elements of V with $s(e) \in B_i$. We computed, for each independent run, the maximum error $\max_{e \in E_i} \{|\widehat{s}(e) - s(e)|\}$ (where $\widehat{s}(e)$ is obtained either with PPS or UNI), and averaged the maximum error over ten independent runs, to obtain the average maximum error ($\bar{\eta}_{B_i}$) and its standard deviation, shown in [Figure 5](#). Note that $\bar{\eta}_{B_i}$ is a very precise metric to capture the local estimation performances, given by the fact that it considers the *maximum error* over each bucket B_i , which can be very large, i.e., at most 2.

From [Figure 5](#) we first observe that both PPS and UNI approaches achieve smaller maximum error ($\bar{\eta}_{B_i}$) for buckets corresponding to elements with higher $s(e)$. Such behavior is likely caused by the fact that for elements with high value of $s(e)$, the difference between $b(e) - a(e)$ (see [Equation \(2\)](#)) is high, hence even rough estimates of terms $W_{C_j}(e)$ yield a good approximation of $s(e)$. The previous observation also explains the larger error over elements with silhouette $s(e)$ close to 0. Comparing the average error $\bar{\eta}_{B_i}$ we observe that, PPS significantly reduces the error (and its standard deviation) over *all* buckets with respect to UNI on most inputs. For example, on the IOT data with d_{can} and $k = 5$ the estimates reported by PPS have half of the maximum error achieved by UNI. Similarly, on the GOW data for $k = 2, t = 32$ the standard deviation of the error of PPS is significantly smaller on each bucket compared to UNI. We observe that on some configurations PPS achieves similar performances to the UNI approach (e.g., GOW for $k = 10$). Nevertheless, we never observed PPS reporting estimates with significantly smaller accuracy compared to UNI, highlighting the high quality of the estimates of PPS as captured by [Theorem 1](#). We provide some additional results in [Section D](#).

5.3.2 Accuracy over clusters

Next we investigate the local approximation error of PPS and UNI across each cluster of \mathcal{C} . That is, for each cluster we computed both the maximum error $\max_{e \in C} \{|\widehat{s}(e) - s(e)|\}$ and the average error $(1/|C|) \sum_{e \in C} |\widehat{s}(e) - s(e)|$ (where $\widehat{s}(e)$ is computed either with UNI or PPS).

In [Figure 6](#), we visualize the maximum and average errors for different input configurations, over ten independent runs. We observe the PPS method reports estimates with comparable or

⁹The bucket corresponding to index $i = 40$ also contains the right endpoint $L_{40} = 1$.

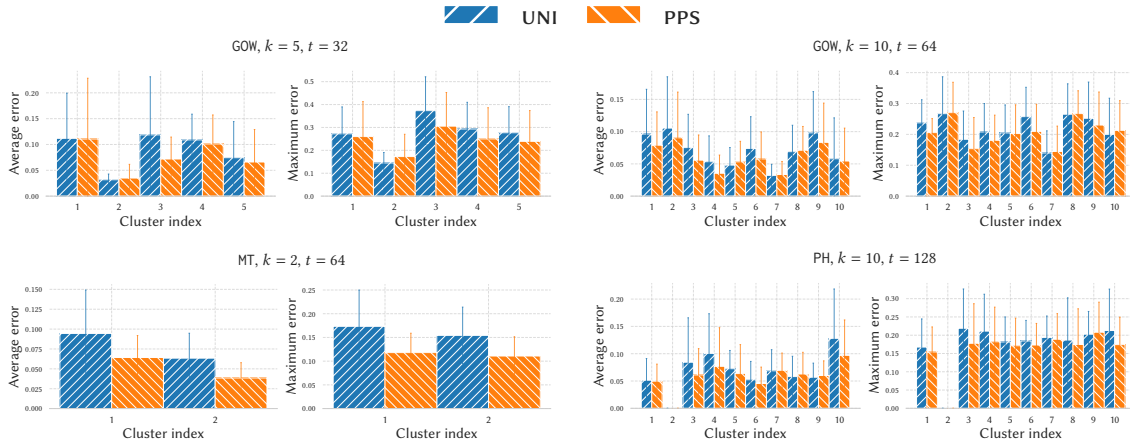


Figure 6: Plots of the average and maximum errors within each cluster achieved by PPS and UNI, over ten independent runs, for various input configurations. Each dot represents a distinct run.

significantly smaller average or maximum error compared to UNI. As an example, on the MT dataset with $k = 2$, the average and maximum errors of PPS for Cluster 1 are respectively bounded by 0.12 and 0.21, while, in contrast, those of UNI are bounded by 0.17 and 0.28, respectively. Similarly, on the GOW dataset with $k = 10$, on all but cluster-index 7, our SILH-PPS-ALL always attains smaller average and maximum errors with respect to UNI. We report additional results in [Section D](#).

Summary for issue I2. We investigated the accuracy for the extremely challenging task of computing the local silhouette value of *all* elements $e \in V$ (i.e., [Problem 1](#)). Our experiments show that our SILH-PPS-ALL algorithm provides highly-accurate estimates for all elements $e \in V$, with significantly reduced variance compared to the UNI baseline. That is, the estimates of PPS are more accurate independently of the actual silhouette values ([Section 5.3.1](#)), and independently of the cluster to which the elements belong ([Section 5.3.2](#)), which are desirable properties for practical applications.

5.4 Distributed implementation

As discussed in [Section 4.3](#), our SILH-PPS-ALL can be efficiently implemented in a distributed setting, such as the one modeled by the MapReduce/MPC frameworks, using a constant number of rounds. In this section, we assess the scalability of this distributed implementation of SILH-PPS-ALL, thus dealing with [Issue I3](#). Since our experiments are performed on a single machine we rely on a simple parallel implementation retaining the steps in [Section 4.3](#) (see [Section C.2](#) for details of the platform used, and [Section C.3](#) for more details on our parallelization strategy).

Our goal is to study the parallel speedup of SILH-PPS-ALL varying the number of threads in $\{2, 4, 8, 16\}$, varying the number of clusters $k \in \{2, 5, 10, 15, 20\}$, and varying $t \in \{512, 1024\}$. We considered our largest datasets from [Table 2](#). For each configuration we perform five runs, and recorded the speedup over the sequential implementation. That is, let T_i be the average time (over the five runs) to execute SILH-PPS-ALL with $i \in \{1, 2, 4, 8, 16\}$ threads, i.e., T_1 is associated with the sequential implementation. We will study the average speedup T_1/T_i .

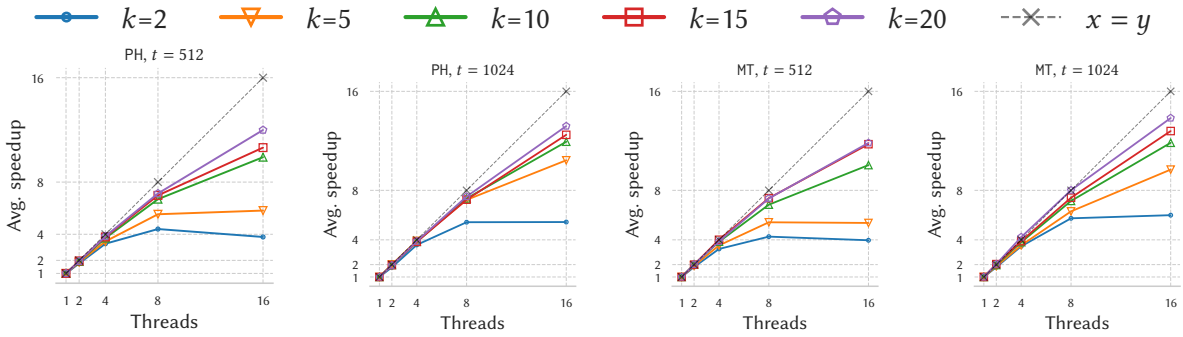


Figure 7: Average parallel speedup over five independent runs by running SILH-PPS-ALL with a parallel implementation. Each configuration shows different values for the sample size t .

The results are reported in Figure 7. We observe a remarkable speed-up over the sequential implementation of the parallel algorithm up to 8 threads on all k values (except for $k = 2$, see discussion below). More specifically, SILH-PPS-ALL achieves an almost linear speedup using up to 8 threads. The speedup becomes slightly smaller than linear for a larger number of threads, which is expected due to the increased overhead introduced by synchronization. Next, we observe that the parallel speedup is significantly greater for larger values of k and t , since our implementation parallelizes the work over different clusters in C (see Section C.3). That is, for smaller values of k and t the degree of parallelism in the computation is not sufficient to compensate the overheads incurred by the multi-threaded implementation, i.e., synchronization. Finally, we note that a larger value of t leads to a higher speedup (e.g., on MT with $t = 1024$ the speedup with 16 threads is about 14 for $k = 20$). Remarkably, when using $t = 1024$ on PH with $k \geq 5$ and 16 threads, we obtain a speedup of at least $10\times$ compared to the sequential execution of SILH-PPS-ALL. Notably, over such configuration, our parallel implementation of SILH-PPS-ALL computes extremely accurate estimates in less than 30 seconds (see Table 4 in Section D, and recall that the PH dataset cannot be processed by the exact algorithm even within hours).

Summary for issue I3. A simple distributed implementation of SILH-PPS-ALL achieves remarkable speedups over its sequential version. The parallel speedup and the high accuracy achieved by SILH-PPS-ALL enable the estimation of the silhouette of all elements of massive datasets. That is, our method enables an extremely efficient processing of datasets that cannot be analyzed through current (sequential) methods.

5.5 Applications

5.5.1 Silhouette plot construction

We now show that the local estimates in output to SILH-PPS-ALL can be used to build a silhouette plot of a clustering C that closely matches the exact one (e.g., see an example of silhouette plot in Figure 1b). In this setting, we focus on BR, our smallest dataset, for ease of visualization,¹⁰ and for the fact that we can compute the exact values of $s(e)$, for all $e \in V$.

¹⁰To avoid cluttered plots, it is good practice to visualize only a small subset of the elements of V over silhouette plots; even on large datasets.

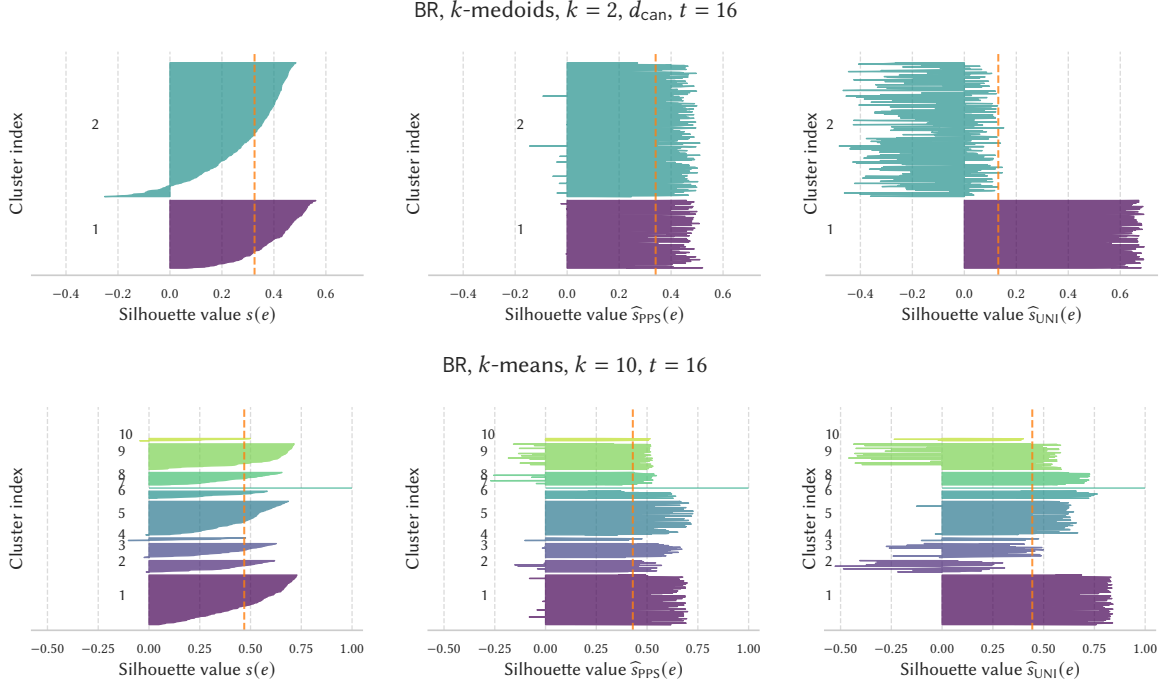


Figure 8: Silhouette plot construction. (Left): Silhouette plot obtained from the exact algorithm. (Center): Silhouette plot obtained by SILH-PPS-ALL, where elements are ordered according to the Left plot. (Right): Silhouette plot obtained by UNI, where elements are ordered according to the Left plot. For all plots, the dashed line represents the average value, computed over all elements.

Figure 8 reports an example of two clusterings C , obtained respectively with k -medoids (top) and with k -means (bottom). In the top panel, we observe that the estimates provided by SILH-PPS-ALL are generally more accurate than those provided by UNI, whose estimates are rather far from their actual values, especially for Cluster 2. In the bottom panel, we first note that both SILH-PPS-ALL and UNI provide similar values for the estimate of the global silhouette coefficient $s(C)$ (dashed line). Interestingly, the two methods yield rather different silhouette plots. Namely, the plot obtained with the estimates of SILH-PPS-ALL is much closer to the one obtained with the exact algorithm. For example, the estimates of SILH-PPS-ALL on Cluster 1 never exceed 0.75, in contrast with UNI, whose estimates can be larger than 0.8 (note that the exact values for Cluster 1 are all less than 0.75). Similarly, for Cluster 9, SILH-PPS-ALL assigns negative values to very few elements as opposed to UNI.

5.5.2 Selection of the best value of k

Let V be a dataset and let $K = \{k_1, \dots, k_{|K|}\}$ be a set containing different values of k used to cluster V . The global silhouette is often used to select the value of $k \in K$ that yields the best clustering for V . Specifically, for each $k \in K$ we obtain a clustering C_k (e.g., using k -means) and select C_{k^*} as the best clustering for V , where $k^* = \arg \max_{k \in K} s(C_k)$ [Shahapure and Nicholas, 2020]. In this subsection we compare the effectiveness of GL-PPS-S versus GL-UNI-S in detecting the best value of k to be used for clustering. We focus on these two estimators, since, as argued before,

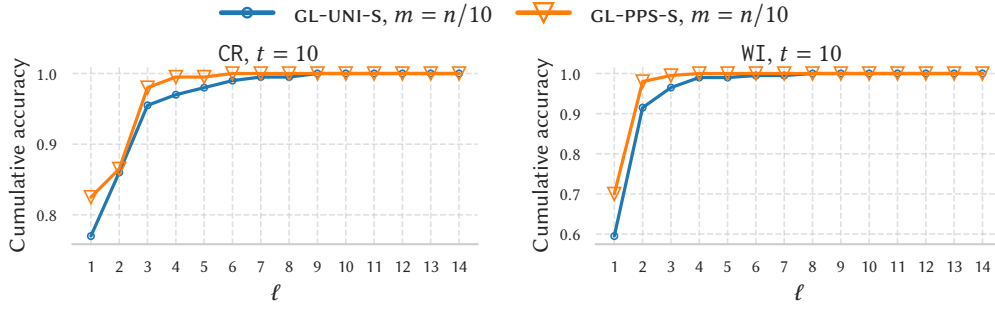


Figure 9: Plots of Cumulative accuracy($\ell, \widehat{\mathbf{k}}$), where $\ell \in [1, 14]$ and $\widehat{\mathbf{k}}$ is either \mathbf{k}^{PPS} or \mathbf{k}^{UNI} . For each value of ℓ , the plots report the cumulative accuracy of each estimation method over 200 runs: values closer to 1, denote a higher accuracy for the identification of the best value of k .

they are accurate and their computation is scalable (see summary for Issue I1 in Section 5.2). Thus, they can be used to compute high-quality approximations of $s(C_k)$ for many different candidate values of k .

We considered two datasets for which we can compute $s(C_k)$ exactly and efficiently, namely CR and WI. We clustered each dataset with k -means, with different values of $k \in K$, with $K = \{2, \dots, 15\}$, and for each resulting clustering C_k we computed the exact global silhouette $s(C_k)$. Then, for each of the two algorithms GL-PPS-S and GL-UNI-S, both run with $m = n/10$ and $t = 10$, we performed $N = 200$ independent runs for each distinct value of k . Let $\widehat{s}(C_k)_j$ be the estimate of either GL-PPS-S or GL-UNI-S on dataset V clustered with value $k \in [2, 15]$ at iteration $j \in [1, N]$. We let $\mathbf{k}^{\text{exact}}$ be the vector of the 14 values of $k \in K$, sorted by non-increasing values of the corresponding global silhouette, that is, $s(C_{\mathbf{k}_1^{\text{exact}}}) \geq s(C_{\mathbf{k}_2^{\text{exact}}}) \geq \dots \geq s(C_{\mathbf{k}_{14}^{\text{exact}}})$. Similarly, we let $\mathbf{k}^{\text{PPS}}(j)$ (resp. $\mathbf{k}^{\text{UNI}}(j)$) denote the vector of the 14 values of $k \in K$, sorted by non-increasing values of the estimates of the corresponding global silhouette provided by GL-PPS-S (resp. GL-UNI-S) in the j -th run, for $j \in [1, N]$. Note that, given a run $j \in [1, N]$ the *best value* of $k \in K$ returned by an approximate method corresponds to $\mathbf{k}_1^{\text{PPS}}(j)$, or $\mathbf{k}_1^{\text{UNI}}(j)$. To assess the accuracy of GL-PPS-S and GL-UNI-S for selecting a reasonable value of $k \in K$ with respect to the exact approach, we now define a *cumulative accuracy* function of each approximate method. Given $\ell \in [1, |K|]$, the cumulative accuracy evaluated at ℓ corresponds to the fraction of runs in which the approximate method selects as best value $k \in K$ a value in the top- ℓ positions of $\mathbf{k}^{\text{exact}}$ (i.e., $k \in \{\mathbf{k}_1^{\text{exact}}, \dots, \mathbf{k}_\ell^{\text{exact}}\}$). More formally given the set of N sorted vectors $\widehat{\mathbf{k}}(j)$, where $\widehat{\mathbf{k}}(j)$ is either $\mathbf{k}^{\text{PPS}}(j)$ or $\mathbf{k}^{\text{UNI}}(j)$, $j \in [1, N]$, the cumulative accuracy corresponds to,

$$\text{Cumulative accuracy}(\ell, \widehat{\mathbf{k}}) \doteq \frac{1}{N} \sum_{j=1}^N \sum_{i=1}^{\ell} \mathbf{1} \left[\widehat{\mathbf{k}}_1(j) = \mathbf{k}_i^{\text{exact}} \right].$$

Where $\mathbf{1}[\cdot]$ corresponds to the indicator function. Observe that, as a function of ℓ , the cumulative accuracy eventually hits the value of 1 for $\ell = |K|$. Clearly, a function approaching 1 very quickly indicates that the associated estimation method features high precision and a small variance in selecting a good value of k , according to $\mathbf{k}^{\text{exact}}$.

Results are reported in Figure 9, where we observe that the GL-PPS-S method has significantly higher accuracy than GL-UNI-S. For example, more than 97% of the 200 runs of GL-PPS-S yield

the selection as best value of k one of the top-3 values in $\mathbf{k}^{\text{exact}}$ on dataset CR, and one of the top-2 values in $\mathbf{k}^{\text{exact}}$ on the WI dataset. In contrast, GL-UNI-S achieves smaller accuracy: less than 95% of the 200 runs correctly yield the selection of one the top-3 values of k in $\mathbf{k}^{\text{exact}}$ on the CR and less than 92% of the runs detect one of the top-2 values in $\mathbf{k}^{\text{exact}}$ on the WI dataset. We observe that the global accuracy is affected by how the exact silhouette values vary across the top- ℓ elements of $\mathbf{k}^{\text{exact}}$ (we show the ordering of $\mathbf{k}^{\text{exact}}$ in Table 5). For example, in the above experiments the silhouette values associated with the top-2 values of $\mathbf{k}^{\text{exact}}$ do not differ much, making the detection of the *best* k extremely challenging, especially for GL-UNI-S.

Summary for issue I4. We studied two different and widely adopted applications of the silhouette coefficient. First, we showed that the local estimates of SILH-PPS-ALL can be used to approximate the silhouette plots of a clustering C , matching exact plots. Second, we showed that our algorithm GL-PPS-S for global silhouette estimation can be safely used in lieu of the expensive exact algorithm to detect the best clustering granularity (i.e., the value k yielding higher $s(C_k)$) for a given dataset V , improving over existing methods. Our experiments showcase the large applicability of the methods designed in this work for both local and global estimation scenarios.

6 Conclusions

In this work, we introduced an efficient, sampling-based algorithm to estimate the silhouette of *all* elements of a clustered dataset. Our new method (SILH-PPS-ALL), dramatically reduces the quadratic complexity required by the exact computation, while providing quantitative guarantees on the approximation error. In addition, we introduced several efficient estimators for the global silhouette providing a tight characterization of their required sample size.

Finally, we designed a distributed variant of our techniques, which requires small (sublinear) local memory, linear aggregate memory, and a constant number of computation rounds.

We validated our techniques through extensive experiments that show the accuracy, efficiency, and parallel scalability of our new methods for local and global silhouette estimation. For the local silhouette values, we showed that SILH-PPS-ALL provides highly accurate estimates compared to existing (heuristic) methods. For the global silhouette value, we showed that GL-PPS-S (based on SILH-PPS-ALL’s sampling schema) often achieves the best trade-off between number of samples processed and accuracy. That is, GL-PPS-S reports highly accurate estimates with small variance while being extremely efficient. We performed further experiments that showcase the use of our methods for two widespread applications: *i*) the (approximate) construction of silhouette plots; and *ii*) the selection of the best clustering granularity k for a dataset.

These are some open issues deserving further investigation: *i*) devising a more flexible, dynamic version of the algorithm where the desired accuracy can be incrementally refined by reusing (part of) the previously sampled elements; *ii*) designing data-dependent sampling approaches, that adapt their sample complexity to the input datasets; *iii*) extending our methods to other popular clustering validation measures, which we discuss in more detail in Section B.

7 Acknowledgments

This research is funded by the Ministry of University and Research of Italy within the Complementary National Plan PNC-I.1 “Research initiatives for innovative technologies and pathways in the health and welfare sector, D.D. 931 of 06/06/2022, PNC0000002 DARE - Digital Lifelong Prevention CUP: B53C22006440001”. This research is also funded by the ERC Advanced Grant REBOUND (834862), and the Wallenberg AI, Autonomous Systems and Software Program (WASP) funded by the Knut and Alice Wallenberg Foundation.

References

- C. C. Aggarwal and C. K. Reddy, editors. *Data Clustering*. Chapman and Hall/CRC, sep 2014. doi: 10.1201/9781315373515.
- F. Altieri, A. Pietracaprina, G. Pucci, and F. Vandin. *Scalable Distributed Approximation of Internal Measures for Clustering Evaluation*, pages 648–656. Society for Industrial and Applied Mathematics, Jan. 2021. ISBN 9781611976700. doi: 10.1137/1.9781611976700.73.
- O. Arbelaitz, I. Gurrutxaga, J. Muguerza, J. M. Pérez, and I. Perona. An extensive comparative study of cluster validity indices. *Pattern Recognition*, 46(1):243–256, Jan. 2013. ISSN 0031-3203. doi: 10.1016/j.patcog.2012.07.021.
- B. Bahmani, B. Moseley, A. Vattani, R. Kumar, and S. Vassilvitskii. Scalable k-means++. *Proceedings of the VLDB Endowment*, 5(7):622–633, mar 2012. doi: 10.14778/2180912.2180915.
- M. F. Balcan, S. Ehrlich, and Y. Liang. Distributed k-means and k-median clustering on general topologies. *NIPS*, June 2013.
- A. Barger and D. Feldman. k-means for streaming and distributed big sparse data. In *Proceedings of the 2016 SIAM International Conference on Data Mining*. Society for Industrial and Applied Mathematics, jun 2016. doi: 10.1137/1.9781611974348.39.
- P. Beame, P. Koutris, and D. Suciu. Communication steps for parallel query processing. *J. ACM*, 64(6):40:1–40:58, 2017.
- M. Ceccarello, C. Fantozzi, A. Pietracaprina, G. Pucci, and F. Vandin. Clustering uncertain graphs. *Proceedings of the VLDB Endowment*, 11(4):472–484, dec 2017. doi: 10.1145/3186728.3164143.
- M. Ceccarello, A. Pietracaprina, and G. Pucci. Solving k-center clustering (with outliers) in MapReduce and streaming, almost as accurately as sequentially. *Proceedings of the VLDB Endowment*, 12(7):766–778, mar 2019. doi: 10.14778/3317315.3317319.
- S. Chechik, E. Cohen, and H. Kaplan. Average distance queries through weighted samples in graphs and metric spaces: High scalability with tight statistical guarantees. In N. Garg, K. Jansen, A. Rao, and J. D. P. Rolim, editors, *Approximation, Randomization, and Combinatorial Optimization. Algorithms and Techniques, APPROX/RANDOM 2015, August 24-26, 2015*,

Princeton, NJ, USA, volume 40 of *LIPIcs*, pages 659–679. Schloss Dagstuhl - Leibniz-Zentrum für Informatik, 2015. doi: 10.4230/LIPIcs.APPROX-RANDOM.2015.659.

- E. Cohen, S. Chechik, and H. Kaplan. Clustering small samples with quality guarantees: Adaptivity with one2all PPS. In S. A. McIlraith and K. Q. Weinberger, editors, *Proceedings of the Thirty-Second AAAI Conference on Artificial Intelligence, (AAAI-18), the 30th innovative Applications of Artificial Intelligence (IAAI-18), and the 8th AAAI Symposium on Educational Advances in Artificial Intelligence (EAAI-18), New Orleans, Louisiana, USA, February 2-7, 2018*, pages 2884–2891. AAAI Press, 2018. URL <https://www.aaai.org/ocs/index.php/AAAI/AAAI18/paper/view/17084>.
- A. Czumaj, G. Gao, M. Ghaffari, and S. H. Jiang. Fully scalable MPC algorithms for euclidean k -center. In *Proceedings of the 52nd International Colloquium on Automata, Languages, and Programming, ICALP 2025*, volume 334 of *LIPIcs*, pages 64:1–64:20, 2025.
- J. Dean and S. Ghemawat. MapReduce. *Communications of the ACM*, 51(1):107–113, jan 2008. doi: 10.1145/1327452.1327492.
- D.-T. Dinh, T. Fujinami, and V.-N. Huynh. *Estimating the Optimal Number of Clusters in Categorical Data Clustering by Silhouette Coefficient*, pages 1–17. Springer Singapore, 2019. ISBN 9789811512094. doi: 10.1007/978-981-15-1209-4_1.
- D. P. Dubhashi and A. Panconesi. *Concentration of Measure for the Analysis of Randomized Algorithms*. Cambridge University Press, Cambridge, UK, 2009. ISBN 978-0-521-88427-3.
- A. Dudek. *Silhouette Index as Clustering Evaluation Tool*, pages 19–33. Springer International Publishing, 2020. ISBN 9783030523480. doi: 10.1007/978-3-030-52348-0_2.
- A. Ene, S. Im, and B. Moseley. Fast clustering using MapReduce. In *Proceedings of the 17th ACM SIGKDD international conference on Knowledge discovery and data mining - KDD '11*. ACM Press, 2011. doi: 10.1145/2020408.2020515.
- D. Feldman and M. Langberg. A unified framework for approximating and clustering data. In *Proceedings of the 43rd annual ACM symposium on Theory of computing - STOC '11*. ACM Press, 2011. doi: 10.1145/1993636.1993712.
- G. Frahling and C. Sohler. A Fast k -Means Implementatino Using Coresets. *International Journal of Computational Geometry & Applications*, 18(06):605–625, dec 2008. doi: 10.1142/s0218195908002787.
- J. Han, M. Kamber, and J. Pei. *Data mining: concepts and techniques*. Elsevier, 2011. doi: 10.1016/c2009-0-61819-5.
- B. A. Hassan, N. B. Tayfor, A. A. Hassan, A. M. Ahmed, T. A. Rashid, and N. N. Abdalla. From a-to-z review of clustering validation indices. *Neurocomputing*, 601:128198, Oct. 2024. ISSN 0925-2312. doi: 10.1016/j.neucom.2024.128198.
- C. Hennig, M. Meila, F. Murtagh, and R. Rocci. *Handbook of Cluster Analysis*. CRC PRESS, S.I, 2015. ISBN 9780367570408.

- M. S. Hossain and R. A. Angryk. GDClust: A graph-based document clustering technique. In *Seventh IEEE International Conference on Data Mining Workshops (ICDMW 2007)*. IEEE, oct 2007. doi: 10.1109/icdmw.2007.104.
- E. Hruschka, L. de Castro, and R. Campello. Evolutionary algorithms for clustering gene-expression data. In *Fourth IEEE International Conference on Data Mining (ICDM'04)*. IEEE. doi: 10.1109/icdm.2004.10073.
- A. M. Ikotun, A. E. Ezugwu, L. Abualigah, B. Abuhaija, and J. Heming. K-means clustering algorithms: A comprehensive review, variants analysis, and advances in the era of big data. *Information Sciences*, 622:178–210, Apr. 2023. ISSN 0020-0255. doi: 10.1016/j.ins.2022.11.139.
- S. Im, R. Kumar, S. Lattanzi, B. Moseley, and S. Vassilvitskii. Massively parallel computation: Algorithms and applications. *Foundations and Trends® in Optimization*, 5(4):340–417, 2023.
- H. J. Karloff, S. Suri, and S. Vassilvitskii. A model of computation for mapreduce. In M. Charikar, editor, *Proceedings of the Twenty-First Annual ACM-SIAM Symposium on Discrete Algorithms, SODA 2010, Austin, Texas, USA, January 17-19, 2010*, pages 938–948. SIAM, 2010. doi: 10.1137/1.9781611973075.76.
- G. Karypis and V. Kumar. A fast and high quality multilevel scheme for partitioning irregular graphs. *SIAM Journal on Scientific Computing*, 20(1):359–392, Jan. 1998. ISSN 1095-7197. doi: 10.1137/s1064827595287997.
- L. Kaufmann and P. Rousseeuw. Clustering by means of medoids. *Data Analysis based on the L1-Norm and Related Methods*, pages 405–416, 01 1987.
- J. Kleinberg. An impossibility theorem for clustering. *Advances in neural information processing systems*, 15, 2002.
- H. Lai, T. Huang, B. Lu, S. Zhang, and R. Xiaog. Silhouette coefficient-based weighting k-means algorithm. *Neural Computing and Applications*, 37(5):3061–3075, Dec. 2024. ISSN 1433-3058. doi: 10.1007/s00521-024-10706-0.
- L. Lenssen and E. Schubert. Medoid silhouette clustering with automatic cluster number selection. *Information Systems*, 120:102290, Feb. 2024. ISSN 0306-4379. doi: 10.1016/j.is.2023.102290.
- J. Leskovec, A. Rajaraman, and J. D. Ullman. *Mining of Massive Datasets*. Cambridge University Press, 2014. doi: 10.1017/cbo9781139924801.
- L. Liu, R. Jin, C. C. Aggarwal, and Y. Shen. Reliable clustering on uncertain graphs. In M. J. Zaki, A. Siebes, J. X. Yu, B. Goethals, G. I. Webb, and X. Wu, editors, *12th IEEE International Conference on Data Mining, ICDM 2012, Brussels, Belgium, December 10-13, 2012*, pages 459–468. IEEE Computer Society, 2012. doi: 10.1109/ICDM.2012.11.
- Y. Liu, Z. Li, H. Xiong, X. Gao, and J. Wu. Understanding of internal clustering validation measures. In *2010 IEEE International Conference on Data Mining*. IEEE, Dec. 2010. doi: 10.1109/icdm.2010.35.

- R. Lletí, M. Ortiz, L. Sarabia, and M. Sánchez. Selecting variables for k-means cluster analysis by using a genetic algorithm that optimises the silhouettes. *Analytica Chimica Acta*, 515(1): 87–100, July 2004. ISSN 0003-2670. doi: 10.1016/j.aca.2003.12.020.
- S. Lloyd. Least squares quantization in PCM. *IEEE Transactions on Information Theory*, 28(2): 129–137, mar 1982. doi: 10.1109/tit.1982.1056489.
- L. Lovmar, A. Ahlford, M. Jonsson, and A.-C. Syvänen. Silhouette scores for assessment of snp genotype clusters. *BMC Genomics*, 6(1), Mar. 2005. ISSN 1471-2164. doi: 10.1186/1471-2164-6-35.
- G. Malkomes, M. J. Kusner, W. Chen, K. Q. Weinberger, and B. Moseley. Fast distributed k-center clustering with outliers on massive data. In C. Cortes, N. D. Lawrence, D. D. Lee, M. Sugiyama, and R. Garnett, editors, *Advances in Neural Information Processing Systems 28: Annual Conference on Neural Information Processing Systems 2015, December 7-12, 2015, Montreal, Quebec, Canada*, pages 1063–1071, 2015. URL <https://proceedings.neurips.cc/paper/2015/hash/8fecb20817b3847419bb3de39a609afe-Abstract.html>.
- A. Mazzetto, A. Pietracaprina, and G. Pucci. Accurate mapreduce algorithms for k-median and k-means in general metric spaces. In P. Lu and G. Zhang, editors, *30th International Symposium on Algorithms and Computation, ISAAC 2019, December 8-11, 2019, Shanghai University of Finance and Economics, Shanghai, China*, volume 149 of *LIPIcs*, pages 34:1–34:16. Schloss Dagstuhl - Leibniz-Zentrum für Informatik, 2019. doi: 10.4230/LIPIcs.ISAAC.2019.34.
- M. Mitzenmacher and E. Upfal. *Probability and Computing*. Cambridge University Press, Cambridge, UK, 2nd edition, 2017. ISBN 9781316651124.
- D. Moulavi, P. A. Jaskowiak, R. J. G. B. Campello, A. Zimek, and J. Sander. Density-based clustering validation. In M. J. Zaki, Z. Obradovic, P. Tan, A. Banerjee, C. Kamath, and S. Parthasarathy, editors, *Proceedings of the 2014 SIAM International Conference on Data Mining, Philadelphia, Pennsylvania, USA, April 24-26, 2014*, pages 839–847. SIAM, 2014. doi: 10.1137/1.9781611973440.96.
- R. T. Ng and J. Han. Efficient and effective clustering methods for spatial data mining. In J. B. Bocca, M. Jarke, and C. Zaniolo, editors, *VLDB’94, Proceedings of 20th International Conference on Very Large Data Bases, September 12-15, 1994, Santiago de Chile, Chile*, pages 144–155. Morgan Kaufmann, 1994. URL <http://www.vldb.org/conf/1994/P144.PDF>.
- A. Pietracaprina, G. Pucci, M. Riondato, F. Silvestri, and E. Upfal. Space-round tradeoffs for mapreduce computations. In U. Banerjee, K. A. Gallivan, G. Bilardi, and M. Katevenis, editors, *International Conference on Supercomputing, ICS’12, Venice, Italy, June 25-29, 2012*, pages 235–244. ACM, 2012. doi: 10.1145/2304576.2304607.
- A. Pranjali and M. F. Balcan. Center based clustering: A foundational perspective, 2013.
- P. J. Rousseeuw. Silhouettes: A graphical aid to the interpretation and validation of cluster analysis. *Journal of Computational and Applied Mathematics*, 20:53–65, nov 1987. doi: 10.1016/0377-0427(87)90125-7.

- E. Schubert. Stop using the elbow criterion for k-means and how to choose the number of clusters instead. *ACM SIGKDD Explorations Newsletter*, 25(1):36–42, June 2023. ISSN 1931-0153. doi: 10.1145/3606274.3606278.
- E. Schubert and L. Lenssen. Fast k-medoids clustering in rust and python. *Journal of Open Source Software*, 7(75):4183, 2022.
- E. Schubert and P. J. Rousseeuw. Fast and eager k -medoids clustering: $O(k)$ runtime improvement of the pam, clara, and clarans algorithms. *Information Systems*, 101:101804, Nov. 2021. ISSN 0306-4379. doi: 10.1016/j.is.2021.101804.
- T. Sellam, R. Cijvat, R. Koopmanschap, and M. L. Kersten. Blaeu: Mapping and navigating large tables with cluster analysis. *Proc. VLDB Endow.*, 9(13):1477–1480, 2016. doi: 10.14778/3007263.3007288. URL <http://www.vldb.org/pvldb/vol9/p1477-sellam.pdf>.
- K. R. Shahapure and C. Nicholas. Cluster quality analysis using silhouette score. In *2020 IEEE 7th International Conference on Data Science and Advanced Analytics (DSAA)*, pages 747–748. IEEE, Oct. 2020. doi: 10.1109/dsaa49011.2020.00096.
- P.-N. Tan, M. Steinbach, and V. Kumar. *Introduction to Data Mining*. Pearson Addison Wesley, Boston, 2005. ISBN 9780321321367.
- C. Tomasini, L. R. Emmendorfer, E. N. Borges, and K. S. Machado. A methodology for selecting the most suitable cluster validation internal indices. In S. Ossowski, editor, *Proceedings of the 31st Annual ACM Symposium on Applied Computing, Pisa, Italy, April 4-8, 2016*, pages 901–903. ACM, 2016. doi: 10.1145/2851613.2851885.
- M. Van der Laan, K. Pollard, and J. Bryan. A new partitioning around medoids algorithm. *Journal of Statistical Computation and Simulation*, 73(8):575–584, Aug. 2003. ISSN 1563-5163. doi: 10.1080/0094965031000136012.
- F. Wang, H. Franco-Penya, J. D. Kelleher, J. Pugh, and R. J. Ross. An analysis of the application of simplified silhouette to the evaluation of k-means clustering validity. In P. Perner, editor, *Machine Learning and Data Mining in Pattern Recognition - 13th International Conference, MLDM 2017, New York, NY, USA, July 15-20, 2017, Proceedings*, volume 10358 of *Lecture Notes in Computer Science*, pages 291–305. Springer, 2017. doi: 10.1007/978-3-319-62416-7_21. URL https://doi.org/10.1007/978-3-319-62416-7_21.
- C. Wiwie, J. Baumbach, and R. Röttger. Comparing the performance of biomedical clustering methods. *Nature Methods*, 12(11):1033–1038, sep 2015. doi: 10.1038/nmeth.3583.
- H. Xiong and Z. Li. Clustering validation measures. In C. C. Aggarwal and C. K. Reddy, editors, *Data Clustering: Algorithms and Applications*, pages 571–606. CRC Press, 2013.
- D. Xu and Y. Tian. A comprehensive survey of clustering algorithms. *Annals of Data Science*, 2(2):165–193, June 2015. ISSN 2198-5812. doi: 10.1007/s40745-015-0040-1.

A Technical tools

The next results is a standard tool for data mining and machine learning algorithms, to provide concentration for sums of independent and bounded random variables [Mitzenmacher and Upfal, 2017, Theorem 4.12], and is crucial for the analysis of our estimators.

Theorem 6 (Hoeffding’s bound). *Let X_1, \dots, X_m be independent random variables taking values in $[a, b] \subseteq \mathbb{R}$ such that for all $j \in [1, m]$, $\mathbb{E}[X_j] = \mu$. Then*

$$\mathbb{P} \left[\left| \frac{1}{m} \sum_j X_j - \mu \right| \geq \varepsilon \right] \leq 2 \exp \left(-\frac{2m\varepsilon^2}{(b-a)^2} \right) .$$

The next results (belonging to the large family of bounds known as Chernoff-Hoeffding bounds) are used in the proof of [Theorem 1](#). The form of the bounds that we use is from the textbook by [Dubhashi and Panconesi \[2009, Theorem 1.1\]](#).

Theorem 7 (Chernoff-Hoeffding bounds). *Let X_1, \dots, X_m be independent random variables taking values in $[0, 1]$ and let $X = \sum_{i=1}^m X_i$. Then for any $\varepsilon \in (0, 1)$ it holds that*

$$\mathbb{P} [X \geq (1 + \varepsilon)\mathbb{E}[X]] \leq \exp \left(-\frac{\varepsilon^2}{3}\mathbb{E}[X] \right) \quad \text{and} \quad \mathbb{P} [X \leq (1 - \varepsilon)\mathbb{E}[X]] \leq \exp \left(-\frac{\varepsilon^2}{2}\mathbb{E}[X] \right) .$$

B Estimating other clustering validation measures

Our strategy that estimates the terms $W_{C_j}(e)$, $j \in [k]$, $e \in V$ through the PPS approach can be used to approximate various other measures for internal clustering evaluation. In particular, all those measures that are based on sums of distances between elements of the dataset V . This is the case of measures that consider the *cohesion* (i.e., the average intracluster distance) and the *separation* (i.e., the average intercluster distance) of a clustering C [Tan et al. \[2005\]](#).

More precisely, consider a k -clustering $C = \{C_1, \dots, C_k\}$ and define the cohesion and separation of C as

$$\begin{aligned} \text{Coh}(C) &= \frac{1}{2} \frac{\sum_{j=1}^k \sum_{e', e'' \in C_j} d(e', e'')}{\sum_{j=1}^k \binom{|C_j|}{2}} , \\ \text{Sep}(C) &= \frac{\sum_{1 \leq j_1 < j_2 \leq k} \sum_{e' \in C_{j_1}} \sum_{e'' \in C_{j_2}} d(e', e'')}{\sum_{1 \leq j_1 < j_2 \leq k} (|C_{j_1}| |C_{j_2}|)} , \end{aligned}$$

respectively. These measures have also been used to evaluate the average cluster reliability on networks, where distances correspond to connection probabilities [[Ceccarello et al., 2017](#), [Liu et al., 2012](#)]. We can rewrite the above measures in terms of the sums $W_C(e)$ defined in [Equation \(4\)](#), as follows

$$\text{Coh}(C) = \frac{1}{2} \frac{\sum_{j=1}^k \sum_{e \in C_j} W_{C_j}(e)}{\sum_{j=1}^k \binom{|C_j|}{2}} \quad \text{and} \quad \text{Sep}(C) = \frac{\sum_{1 \leq j_1 < j_2 \leq k} \sum_{e \in C_{j_1}} W_{C_{j_2}}(e)}{\sum_{1 \leq j_1 < j_2 \leq k} (|C_{j_1}| |C_{j_2}|)} .$$

Clearly, highly accurate approximations of terms $W_{C_j}(e), j \in [k], e \in V$ with low relative errors yield approximations with low *relative error* for $\text{Coh}(C)$ and $\text{Sep}(C)$. Specifically, let $\widehat{\text{Coh}}(C)$ and $\widehat{\text{Sep}}(C)$ as the approximation of $\text{Coh}(C)$ and $\text{Sep}(C)$ respectively. Where each approximation is obtained by substituting the term $W_C(e)$ with the value $\widehat{W}_C(e)$ computed within SILH-PPS-ALL. The following result is an immediate consequence of [Lemma 1](#).

Theorem 8. *Let V be a dataset of n elements, and let C be a k -clustering of V . Let $\widehat{\text{Coh}}(C)$ and $\widehat{\text{Sep}}(C)$ be the approximations to $\text{Coh}(C)$ and $\text{Sep}(C)$ respectively based on the values $\widehat{W}_C(e)$ computed within SILH-PPS-ALL for parameters $0 < \epsilon, \delta < 1$, and for a suitable choice of constant $c > 0$ in the definition of the sample size t . Then with probability at least $1 - \delta$*

$$\left| \frac{\widehat{\text{Coh}}(C) - \text{Coh}(C)}{\text{Coh}(C)} \right| \leq \epsilon \quad \text{and} \quad \left| \frac{\widehat{\text{Sep}}(C) - \text{Sep}(C)}{\text{Sep}(C)} \right| \leq \epsilon .$$

C Reproducibility

C.1 Datasets

We consider various datasets from the UCI and SNAP repositories, that are publicly available online.¹¹ We provide a script to download and process each dataset with our code.¹² For the k -means objective we used the implementation from `scikit-learn`,¹³ which uses Lloyd’s algorithm coupled with an initialization obtained through `k-means++`. For the k -medoids objective dataset we used the state-of-the-art approach by [Schubert and Lenssen \[2022\]](#).¹⁴

C.2 Setup

We implemented our algorithms and the baseline methods in C++20, and compiled it under `gcc 9.5.0`, with all optimization flags set. Except otherwise stated, all the experiments were performed single-threaded on a 72-core machine Intel Xeon Gold, running Ubuntu 20.04. To cluster the various datasets, we used Python 3.12.3. For the k -means objective, we used the default implementation from the Scikit-learn library,¹⁵ while for the k -medoids objective we used the `k-medoids` library [[Schubert and Rousseeuw, 2021](#)].¹⁶ Our distributed implementation of SILH-PPS-ALL is done using the OpenMP library for C++, given that our execution is on a single many-core machine.

C.3 Parallel implementation

To parallelize our algorithm SILH-PPS-ALL we rely on the OpenMP library. Our implementation adopts the following parallelization strategy:

¹¹<https://archive.ics.uci.edu/datasets/>, <https://snap.stanford.edu/data/>

¹²<https://github.com/iliesarpe/ScalableSilhouetteComputation>

¹³<https://scikit-learn.org/>

¹⁴<https://pypi.org/project/kmedoids/>

¹⁵<https://scikit-learn.org/stable/>

¹⁶<https://pypi.org/project/kmedoids/>

Table 3: Algorithms compared in our experimental evaluation in [Section 5.2](#), and their required parameters: t is used in Phase 1 of our [Algorithm 1](#); m is used to evaluate the estimators in [Equations \(9\)](#) and [\(10\)](#); while we denote with m' the value of the sample size used to evaluate [Equation \(8\)](#). Both parameters t and m apply to PPS and its uniform Poisson-sampling variant UNI (see [Section 4.1.3](#)).

Algorithm name	t	m	m'
GL-S	✗	✗	✓
GL-PPS-F, GL-UNI-F	✓	✗	✗
GL-PPS-S, GL-UNI-S	✓	✓	✗

Table 4: Average runtime (in seconds) required by the sequential execution of SILH-PPS-ALL (i.e., T_1) under the setting of [Section 5.4](#).

Configuration	$k = 2$	$k = 5$	$k = 10$	$k = 15$	$k = 20$
MT, $t = 512$	35.8	72.5	254.3	392.6	506.8
MT, $t = 1024$	72.8	223.9	525.7	702.9	984.8
PH, $t = 512$	44.4	109.6	356.8	561.0	736.9
PH, $t = 1024$	87.7	354.6	756.3	1075.2	1427.7

- We parallelize the **for** loops in [Line 1](#) of [Algorithm 1](#), inspired by **Round 1** and **Round 2** of our Mapreduce algorithm;
- We parallelize the **for** loop in [Line 1](#) of [Algorithm 1](#), inspired by **Round 3** of our Mapreduce algorithm.

For each of the above parallel loop executions, we perform synchronization on the necessary data-structures, yielding some of the bottlenecks discussed in [Section 5.4](#).

D Additional results

In this section we complement our extensive experimental evaluation, by presenting additional results to those of [Section 5](#).

- In [Figure 10](#) we show, for all the missing large dataset of [Table 2](#). The results of the experiments in [Section 5.2.2](#) that compare the global estimates of the various randomized algorithms.
- In [Figure 11](#) we show additional results for the accuracy of PPS and UNI approaches over various buckets—extending results from [Section 5.3.1](#).
- In [Figure 12](#) we show additional results on the average and maximum error on each cluster C of PPS and UNI for the setting of [Section 5.3.2](#).

Table 5: Values of k ordered by $s(C_k)$ (ordering over $\mathbf{k}^{\text{exact}}$). The setting is from [Section 5.5.2](#).

	CR		WI	
	k	$s(C_k)$	k	$s(C_k)$
$\mathbf{k}_1^{\text{exact}}$	$k = 2$	0.552	$k = 2$	0.51
$\mathbf{k}_2^{\text{exact}}$	$k = 4$	0.463	$k = 3$	0.504
$\mathbf{k}_3^{\text{exact}}$	$k = 3$	0.451	$k = 4$	0.45
$\mathbf{k}_4^{\text{exact}}$	$k = 5$	0.419	$k = 5$	0.418
$\mathbf{k}_5^{\text{exact}}$	$k = 7$	0.391	$k = 6$	0.392
$\mathbf{k}_6^{\text{exact}}$	$k = 6$	0.387	$k = 7$	0.367
$\mathbf{k}_7^{\text{exact}}$	$k = 8$	0.38	$k = 8$	0.357
$\mathbf{k}_8^{\text{exact}}$	$k = 10$	0.364	$k = 9$	0.342
$\mathbf{k}_9^{\text{exact}}$	$k = 9$	0.343	$k = 10$	0.334
$\mathbf{k}_{10}^{\text{exact}}$	$k = 11$	0.336	$k = 11$	0.329
$\mathbf{k}_{11}^{\text{exact}}$	$k = 15$	0.333	$k = 12$	0.326
$\mathbf{k}_{12}^{\text{exact}}$	$k = 14$	0.314	$k = 14$	0.325
$\mathbf{k}_{13}^{\text{exact}}$	$k = 12$	0.312	$k = 15$	0.325
$\mathbf{k}_{14}^{\text{exact}}$	$k = 13$	0.304	$k = 13$	0.323

- In [Table 4](#) we show the average sequential runtime required by SILH-PPS-ALL considering the setting of [Section 5.4](#).
- In [Table 5](#) we show the values of $s(C_k)$ for each $k \in \mathbf{k}$ under the setting of [Section 5.5](#).

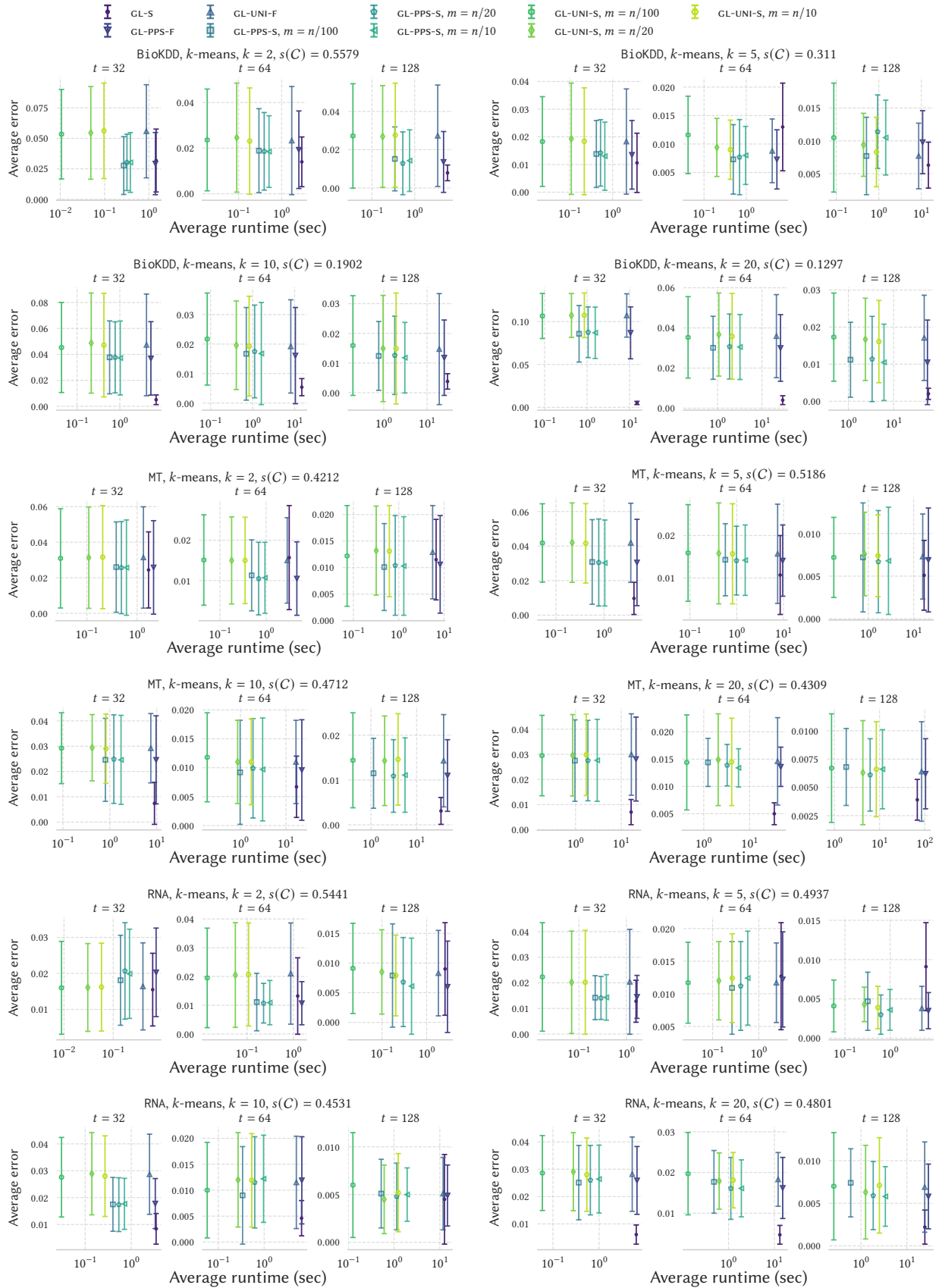


Figure 10: Methods comparison. The x axis is associated with the average runtime, and the y axis with the average error (and its standard deviation) over 10 independent runs. For each clustered dataset we considered different values of the expected sample size $t \in \{32, 64, 128\}$, as illustrated.

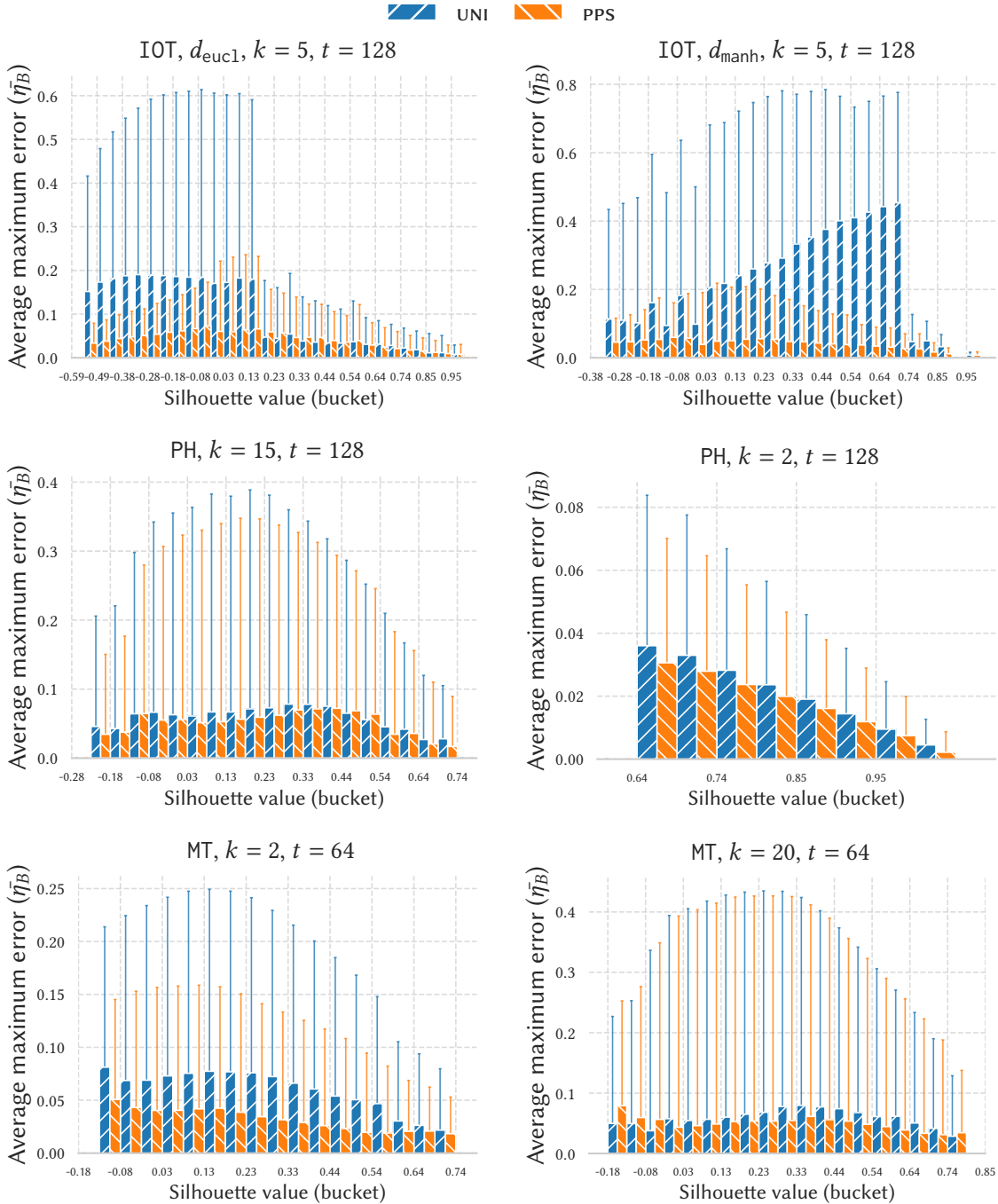


Figure 11: Plots of the average maximum error and its standard deviation obtained on all elements $e \in V$, grouped by bucket, for PPS and UNI, over four configurations. When we report the distance, it indicates that the dataset has been clustered with k -medoids. For ease of visualization we only display the average maximum error over non-empty buckets.

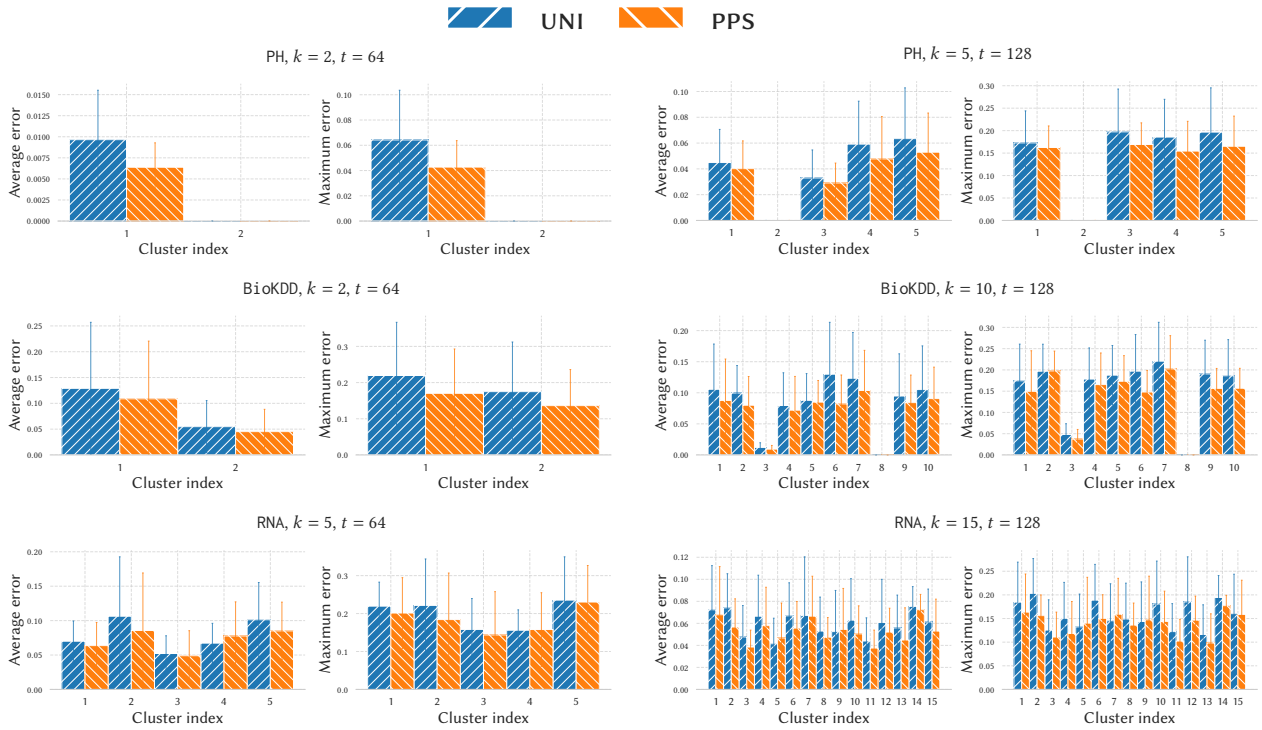


Figure 12: For each cluster in C we show the average and maximum errors achieved by SILH-PPS-ALL (PPS) and the uniform sampling based approach from Section 4.1.3 (UNI). Each dot represent an independent run.